# Warming and greening exacerbate the propagation risk from meteorological to soil moisture drought

**Yifei Li[a], Shengzhi Huang[a,*], Hao Wang[b], Qiang Huang[a], Pei Li[a], Xudong Zheng[a], Zhixia Wang[a], Shijie Jiang[c], Guoyong Leng[d], Ji Li[d], Jian Peng[e]**

a State Key Laboratory of Eco-hydraulics in Northwest Arid Region of China, Xi'an University of Technology, Xi'an 710048, China

b State Key Laboratory of Simulation and Regulation of Water Cycle in River Basin, China Institute of Water Resources and Hydropower Research, Beijing 100038, China

c Department of Computational Hydrosystems, Helmholtz Centre for Environmental Research, 04318 Leipzig, Germany

d Key Laboratory of Water Cycle and Related Land Surface Processes, Institute of Geographic Sciences and Natural Resources Research, Chinese Academy of Sciences, Beijing 100101, China

e Department of Remote Sensing, Helmholtz Centre for Environmental Research−UFZ, Permoserstrasse 15, 04318 Leipzig, Germany

[*] Corresponding author at: State Key Laboratory of Eco-hydraulics in Northwest Arid Region of China, Xi'an University of Technology, Xi'an 710048, China. Tel.: +86 29 82312801; fax: +86 29 82312797. E-mail Address: huangshengzhi7788@126.com.

**Abstract:** Quantifying the propagation time (PT) and trigger threshold (TR) from meteorological to soil moisture drought is critically important for drought early warning and precise defense. Nevertheless, existing propagation characteristics usually have a low temporal-spatial resolution, and their dynamics and related driving mechanisms (such as global warming and greening) are still incompletely understood. To fill the knowledge gap, this study proposes a drought propagation model based on the Bayesian causal analysis framework for quantifying the PT and TR with a high resolution. Taking Northeast China (NEC) as a case study, we further explore the dynamics of drought propagation characteristics in recent decades and possible driving mechanisms using the sliding window and Random Forest model. Results showed that: (1) the drought PT varies spatially and temporally in the study area, with long PT in the central plain and western high-altitude areas in the early growing season (typically over 200 days), while short in the middle and late growing season in most regions (less than one month in July and August), The TR is generally lower than 80mm in the western regions and do not change significantly with time; (2) the PT and TR in the vast central and western regions exhibit a downward trend in the late growing season, resulting in a strikingly increased risk of drought propagation; (3) Increasing vapor pressure deficit (VPD) due to warming, along with decreasing aridity index (AI) due to precipitation shortage are the main drivers on the accelerated drought propagation. Moreover, local greening has also played a critical role in accelerating propagation via transpiration that consumes soil water, which contributes more than 20% to propagation dynamics. Overall, this study sheds new insights into

drought propagation dynamics and mechanisms in a changing environment, providing a promising avenue for drought early warning and mitigation.

**Keywords:** meteorological drought; soil moisture drought; propagation time and trigger threshold; propagation dynamics and mechanism; warming and greening; drought early warning

# 1 Introduction

Drought is an extreme water shortage phenomenon in the process of terrestrial hydrological cycle, which is usually hidden and difficult to forecast in advance (Mishra and Singh, 2011). In many cases, drought can be hardly realized until it has caused considerable losses to the ecological environment, agricultural production and social economy (Chen et al., 2022; Mahecha et al., 2022; Yao et al., 2022; Zhao and Wang, 2021). According to the affected objects, drought is generally classified into four categories: meteorological drought (i.e., rainfall deficit), agricultural drought (i.e., soil moisture deficit), hydrological drought (i.e., abnormal reduction of river streamflow) and socio-economic drought (i.e., imbalance of water supply and demand affecting economic development) (Zhang et al., 2022). Typically in nature, different types of drought rarely occur in isolation in the hydrological cycle, and their causative relationships are often entwined (Van Loon, 2015; Zhang et al., 2022). Drought signal generally starts from the abnormal decrease of precipitation (Mishra and Singh, 2010). For example, with the precipitation deficit persists, soil moisture stored in the early stage will be continuously dissipated by evapotranspiration, then the soil moisture

drought may be triggered. If the precipitation cannot be replenished in time, the drought signal may continue to propagate downward along the hydrological cycle, and eventually resulting in hydrological drought or even groundwater drought (Kumar et al., 2016; Tijdeman et al., 2022; Vicente-Serrano et al., 2020). The process of drought signals transmitting along the hydrological cycle is known as drought propagation (Apurv et al., 2017; Zhang et al., 2021a). Developing a holistic understanding of the propagation process of drought signals in the hydrological cycle system can reveal the formation principle of drought and provide a new path for drought early warning (Li et al., 2022).

In general, meteorological drought is the precursor of other types of droughts, but the shortage of precipitation usually does not lead to other drought types immediately. There are obvious time accumulation and threshold effects in the evolution of drought. Taking meteorological to soil moisture drought as an example, the drought signal needs to continue for a period of time after the onset of meteorological drought to accumulate the shortage of precipitation. When this precipitation deficiency beyond a certain threshold, it may lead to a decrease in soil moisture, thereby triggering soil moisture drought. The time and threshold effects in the process of drought development are generally defined as drought propagation time (PT) and triggering threshold (TR) (Tijdeman et al., 2022; Wu et al., 2021). Having advance knowledge of the drought propagation characteristics (PT and TR) in a particular region is crucial for local water resource managers to timely understand the development status and severity of drought, estimate the amount of water resources required to alleviate it,

and determine when to take appropriate measures (Han et al., 2021). These key pieces of information are vital for early warning and risk management of drought.

In recent years, the propagation between different types of droughts has received increasing attention in the hydrological community (Apurv et al., 2017; Zhang et al., 2021). Earlier studies on the drought propagation commonly employed a relatively simple correlation coefficient method to identify and analyze the general relationship between different drought types (Barker et al., 2016; Huang et al., 2017; López-Moreno et al., 2013). For example, the PT of meteorological drought to hydrological drought can be determined by using the cumulative scales of the Standardized Precipitation Index (SPI) that corresponds to the maximum correlation coefficient between different cumulative scales of SPI and the Standardized Streamflow Index (SSI) (Huang et al., 2017). In subsequent studies, the run theory was usually used to extract drought events in drought index series, and then identified the propagation process between droughts by matching different types of drought events (Bevacqua et al., 2021; Wu et al., 2018). However, the data length can limit the number of drought events that may be finally matched. Recently, some studies employed probability-based methods to estimate the probability of soil moisture drought caused by meteorological drought and further analyzed the relationship between different types of droughts (Xu et al., 2021; Zhu et al., 2021). Additionally, hydrological models have also been used to investigate the propagation of droughts at the basin scale. Such methods have a sound physical basis (Zhang et al., 2021), and can simulate the changes in hydrological variables for analyzing how drought signals propagate. In

spite of these, the models often involve many parameters to be estimated and may suffer from the equifinality issue for different parameters, which complicates their usage. Furthermore, the quality and length of data in many regions are often insufficient to meet the requirement of the models, which also hinders their practical applications (Konapala and Mishra, 2020; Melsen and Guse, 2019; Zhang et al., 2022).

These studies have provided valuable insights that improved our understanding of drought propagation processes in the hydrological cycle and the formation mechanism of drought disasters, but the research on drought propagation is still in the initial stage. In the process of drought propagation, PT and TR are two important characteristics determining whether or not the drought signal propagates downward, and as well as the key parameters for early warning and drought prevention (Guo et al., 2020). However, most of the current studies focus on the calculation and analysis of the PT between different droughts, while the drought TR, which indicates the precipitation deficit required for drought signal transmission, remains unclear. In addition, most of the current research investigated drought propagation processes only at the seasonal scale. However, quantitative studies for the months of the growing season are rare, and the unit of the PT is typically measured on a monthly scale, so the temporal resolution needs to be improved to meet the application requirements (Li et al., 2022). Furthermore, it is remains unclear whether the fluctuation of regional water and energy conditions in a warming climate will change the drought propagation process (especially in the cold regions of higher latitudes) (Peng et al., 2019). As a component of the terrestrial ecosystem, vegetation plays a significant role in the water and energy

exchange between land and atmosphere (Bonan, 2008; Cheng et al., 2022; Seneviratne et al., 2010), and is a bridge to connect and regulate the soil moisture-atmosphere feedback process (Li et al., 2018; Zhao et al., 2022). Therefore, it will be necessary to investigate whether the dynamic change of vegetation (especially in the greening regions) will exacerbate the propagation of drought signals between meteorology and soil moisture (Guo et al., 2023). In the absence of studies addressing these topics, the driving mechanisms of drought propagation under changing environments remain largely unknown.

Northeast China (NEC) is the main production base of corn, soybean and animal husbandry in China, which has an important impact on food security in China and even the world (Wan et al., 2022). In addition, NEC is also rich in forest resources. It is one of the major carbon sink areas in China and has important ecological functions (Ge et al., 2022). However, under the background of global warming, due to the relatively high latitude of NEC, the temperature in this region has risen significantly in recent decades (Zhang et al., 2022), and the drought has shown an increasing trend (Guo et al., 2017; Zhao et al., 2020). This will bring unprecedented challenges to agricultural production and ecological environment protection in NEC (Li et al., 2022).

To sum up, in order to effectively warn against soil moisture drought, this study attempts to address the following three scientific questions: (1) How to effectively estimate the temporal and spatial distribution of drought PT and TR throughout the

150 growing season; (2) How PT and TR respond to the warming and greening contexts;
151 (3) Which factors dominate the drought propagation dynamics and what the
152 propagation mechanisms that drive drought signals are. Taking NEC as the study area,
153 the study used the SPI and standardized soil moisture index (SSMI) to characterize
154 meteorological and soil moisture drought respectively. Based on the proposed drought
155 propagation evaluation framework, five Cupula functions were utilized to establish
156 the connection between precipitation and soil moisture, and the PT and TR required
157 for soil moisture drought at various grades were extracted with a ten-days resolution.
158 We further investigated the dynamic trend of drought propagation characteristics
159 using a sliding window, and the important influencing factors were determined by
160 using a Random Forest model. Finally, the driving mechanisms behind of drought
161 propagation processes under changing environment were analyzed. Overall, this study
162 is expected to provide a scientific basis for drought early warning and drought disaster
163 management.

164 The rest of this paper is organized as follows, Section 2 will introduce the overview
165 of the study area and show the basic information of the data used, and Section 3 will
166 explain the principle and procedure of the method used in this study; then Section 4
167 will show and analyze the results obtained; Section 5 is the discussion part; and
168 finally the main conclusions of this paper will be given in Section 6.

169 # 2 Study area and data

170 ## *2.1 Study area*

Northeast China (NEC) is located in the northeast of the Eurasian continent (115° 52′-135°09′E, 38°40′-53°56′). It covers four provinces and cities with a total area of about 1.25 million $km^2$. Topographically, NEC features a plain surrounded by mountains on its three sides. In the middle of the study area is the Northeast Great Plain, which consists of Sanjiang Plain, Songnen Plain and Liaohe Plain. The Great Plain is surrounded by the Greater Khingan Mountains in the west, the Lesser Khingan Mountains in the north, and the Changbai Mountains in the east (Fig1(a)). The NEC has a temperate continental monsoon climate, which is warm and rainy in summer and cold and long in winter. From south to north, it crosses the middle temperate zone and the sub-frigid zone, where the annual average temperature drops from 11.7°C to -5°C. From east to west, the NEC crosses semi-humid, semiarid and arid areas, with the annual total precipitation gradually declining from 1000mm to less than 200mm (Fig1(b)). As the third largest black soil belt in the world, the Northeast Great Plain is rich in organic matter, with the total grain output accounting for more than 1/5 of the country (Wan et al., 2022). In addition, the mountains surrounding the plain are the largest distribution area of natural forests in China (Fig1(c)) (Ge et al., 2022). The high forest coverage can prolong ice and snow melting, which boosts local agriculture and forestry due to the forest snow storage. However, climate change has considerably increased the temperature (Zhang et al., 2022), and exacerbated drought in NEC over the recent decades (Guo et al., 2017; Zhao et al., 2020), which is extremely unfavorable for rainfed agriculture in the region.

193

194

195 ----------

196 Place **Fig. 1** here.

197 **Fig. 1.** (a) The topography and elevation of the NEC. (b) The spatial distribution of

198 annual average precipitation in the NEC. (c) Terrestrial ecosystems distributed in the

199 study area.

200 ----------

201 ***2.2 Dataset***

202 This study mainly used the long time series of precipitation and soil moisture data

203 from 1962 to 2014 to establish the relationship between meteorological drought and

204 soil moisture drought. The daily gridded precipitation is from the China National

205 Meteorological Information Center (http://www.cma.gov.cn/2011qxfw/2011qsjgx/),

206 which was produced by 2472 national meteorological observation stations by spatial

207 interpolation, with a resolution of 0.5 ° × 0.5 °. This dataset has been widely verified

208 as reliable and extensively used in the monitoring and evaluation of regional drought

209 (Fang et al., 2019). Monthly soil moisture data were derived from Global Land Data

210 Assistance System Version 2 (GLDAS-2.0) (https://disc.gsfc.nasa.gov/), with a spatial

211 resolution of 0.25 ° × 0.25 °. This dataset has been verified in many regions of China

212 as well, providing reliable soil moisture data for agricultural drought research (Wang

213 et al., 2016; Zhang et al., 2017; Zhang et al., 2021). In addition, the potential

214 evapotranspiration (PET) and vapor pressure deficit (VPD) were calculated using the

meteorological variables (such as temperature, pressure, wind speed, radiation, and relative humidity) in the GLDAS-2.0 dataset (1962-2014), which were likewise widely applied in China (Han et al., 2021a; Li et al., 2022). Besides, we used the NDVI index (1981-2014) provided by the Global Inventory Monitoring and Mapping System (GIMMS-NDVI3g) (https://ecocast.arc.nasa.gov/data/pub/gimms/3g.v0) to analyze the impact of vegetation cover change on drought evolution in recent decades. In this study, monthly soil moisture and meteorological data with $0.25° \times 0.25°$ resolution and monthly NDVI data with 8 km ×8 km resolution were upscaled to 0.5° ×0.5° in order to match the spatial resolution of the precipitation dataset.

# 3 Methods

Fig. 2 illustrates the method framework of this paper, which consists of five main procedures: (1) calculating the standardized meteorological and soil moisture drought index, (2) establishing the relationship between soil moisture and precipitation, (3) quantifying the PT of soil moisture drought at different magnitudes, (4) quantifying the drought TR, and (5) driving force analysis of the possible trend in drought propagation characteristics. The details of the method framework are explained as follows.

---

Place **Fig. 2** here.

**Fig. 2.** The framework of identification methods for the drought propagation process.

---

## *3.1 Standardized drought indices*

In recent decades, many drought indicators have been proposed, among which the standardized drought indices constructed on the template of SPI have developed the most rapidly (Zhang et al., 2022). The principle of constructing such indices is to fit specific hydrological variables (e.g., precipitation, runoff and soil moisture) through appropriate probability distribution functions (e.g., Gamma and Gaussian distribution). After calculating the probability of each hydrological variable value under the target cumulative scale, the corresponding drought indices can be finally obtained through standard normalization of the probability values (Han et al., 2021a). This approach was first proposed by (McKee et al., 1993), and compared with traditional drought indicators (such as PDSI), these indices have variable time scales, allowing drought conditions to be evaluated flexibly on monthly, seasonal, or annual scales in accordance with the needs (Fang et al., 2019). In addition, due to the standardized processing, the indices are spatiotemporal comparable, and the calculation is also relatively straightforward with fewer data requirements. Because of these advantages, drought indices developed with this principle (e.g., SPI, SPEI, SSMI, and SSI) have gained widespread use in drought research worldwide (Bevacqua et al., 2021; Choudhury et al., 2021; Kalisa et al., 2020; Peng et al., 2020; Zhao et al., 2020). The SPEI is a drought index established based on the water balance of a certain region (the difference between potential evapotranspiration and actual precipitation). The main advantage of this index is that it can comprehensively consider the meteorological drought development status of a certain region from both precipitation and potential evaporation aspects, however the theme of this study is to establish a direct

relationship between atmospheric precipitation and soil moisture, and further investigate the propagation process of meteorological drought to soil moisture drought. In addition, the soil moisture drought triggering threshold calculated in this article is also expressed by the degree of actual precipitation deficit. Therefore, in characterizing meteorological drought, this article uses the SPI index which can directly reflect the surplus or deficit of precipitation, while considering potential evapotranspiration as an important driving factor in the drought propagation process.

Then SSMI was used to characterize soil moisture drought. A ten-days cumulative unit was used as the minimum cumulative unit in calculating the SPI index for every month during the growing season (i.e., May to September) on the time scale of 1-36 ten-days. By establishing the relationship between SPI at different cumulative scales and SSMI at monthly scales, the propagation characteristics from meteorological drought to soil moisture drought are further estimated (see Section 3.2). Here the calculation steps of SPI and SSMI will be skipped, which can be referred to (Han et al., 2021a; Li et al., 2022) for more details. The grading criteria for standardized drought indices are shown in Table 1.

---

Place **Table. 1** here.

**Table. 1.** Drought classification standard of SPI and SSMI

---

After obtaining the standardized drought indices, in order to the preparation for the next step to establishing the joint distribution between precipitation and soil moisture,

we calculated the Pearson correlation coefficients between the SPI and SSMI in respective scales (Eq. (1)), to analyze the spatial and temporal distribution of the dependence of soil moisture on the precipitation series at different scales.

$$r_{ij} = corr\left(SPI_{ij}, SSMI_{j}\right) \tag{1}$$

where $i$ denotes the cumulative scale of SPI ($i$=1,2, ..., 36 ten-days), $j$ denotes the month in the growing season (from May to September), and $r_{ij}$ is the Pearson correlation coefficient between the monthly scale SSMI series in month $j$ and SPI series with accumulated scale of $i$ ten-days.

### *3.2 Quantification of drought propagation time and trigger threshold*

#### *3.2.1 Constructing joint distribution based on the Copula theory*

How to construct a multidimensional joint distribution is the premise and core of studying the interdependent structure of hydrological variables. Traditionally, the joint distribution functions were built through multidimensional probability distributions (e.g., multidimensional Gaussian distribution or exponential distribution). However, the approach generally demands specific distributions for the marginal distribution of variables, which greatly limits its applicability. The proposal and improvement of Copula function provide a new solution to the above problem (Fang et al., 2019; Wu et al., 2021). Basically, the Copula function is used to describe the multidimensional correlation structure, which connects the marginal distribution functions. Due to unrestricted forms of marginal distribution, as well as the flexibility and diversity of Copula function, this approach has been widely used in the hydrological community

to analyze the relationship between different hydrometeorological variables (Fang et al., 2019; Wu et al., 2021; Zhao et al., 2020).

In this study, five two-dimensional Copula functions commonly used in the field of hydrology (see Table 2) were selected to establish the joint distribution of monthly SSMI and SPI at different time scales. Regardless of which Copular function is used, the joint distribution ( $F_{SPI_i,SSMI}$ ) of SPI and SSMI series is calculated as follows:

$$\begin{aligned} F_{SPI_i,SSMI}\left(spi,ssmi\right) &= P\left(SPI_i < spi, SSMI < ssmi\right) \\ &= C\left(F_{SPI_i}\left(spi\right), F_{SSMI}\left(ssmi\right)\right) \end{aligned} \tag{2}$$

where $F_{SPI_i}$ and $F_{SSMI}$ represent the marginal distribution functions of SPI and SSMI sequences, respectively, *i* denotes the cumulative scale of SPI and its value is 1to36 ten days, *C* is the one of the five Copula functions. In this study, the optimal Copula function for each grid was determined by the least Squared Euclidean Distance (SED).

---

Place **Table. 2** here.

**Table 2.** An overview of the five candidate Copulas

---

### *3.2.2 Identification of the drought propagation time*

The drought PT was determined by the conditional probability of meteorological drought leading to soil moisture drought, which was calculated by a Bayesian causal analysis framework. The specific procedures are as follows:

(1) Firstly, the conditional probability of meteorological drought leading to different

grades of soil moisture drought under different time scales is calculated as follows:

$$P_{ji} = P\left(SSMI_j < ds \mid SPI_{ji} < ds\right) = \frac{P\left(SSMI_j < ds, SPI_{ji} < ds\right)}{P\left(SPI_{ji} < ds\right)} = \frac{C\left(F_{SSMI_j}(ds), F_{SPI_{ji}}(ds)\right)}{F_{SPI_i}(ds)} \quad (3)$$

where *ds* denote different drought grades, the values are -0.5, -1, and -1.5 represent mild, moderate, and severe soil moisture drought scenarios, respectively, $P_{ji}$ indicates the probability of soil moisture drought above *ds* grade caused by meteorological drought with a cumulative scale of *i* (ten-days) in month *j*, *C* represents the joint distribution function using the optimal Copula function.

(2) Based on the probability value ( $P_{ji}$ ) calculated by Eq. (3), the drought propagation probability matrix $P_m$ as follows:

$$P_m = \begin{bmatrix} P_{1,36} & P_{2,36} & P_{3,36} & P_{4,36} & P_{5,36} \\ \vdots & \vdots & \vdots & \vdots & \vdots \\ P_{1,2} & P_{2,2} & P_{3,2} & P_{4,2} & P_{5,2} \\ P_{1,1} & P_{2,1} & P_{3,1} & P_{4,1} & P_{5,1} \end{bmatrix} \quad (4)$$

where each row of the matrix represents the probability of causing soil moisture drought at one of the 36 (ten-days) accumulation scales, and each column represents one of the five months in the growing season (i.e., from May to September). Fig. 3 schematically illustrates the calculation of the probability matrix. Then a probability threshold (PI) is selected to determine the PT from the probability matrix. If the matrix contains a probability greater than the threshold,

the meteorological drought cumulative scale *i* that first reaches the threshold will be regarded as the PT from meteorological drought to soil moisture drought (PT=*i*). Here the threshold is configured as 0.6, and the details will be discussed in Section 5.2.

---

Place **Fig. 3** here.

**Fig. 3.** Schematic diagram of probability matrix calculation steps.

---

### *3.2.3 Quantifying drought trigger threshold*

Based on obtaining the PT, TR (i.e., the total amount of precipitation deficit required to trigger soil moisture drought within the duration of a continued water shortage period of PT) can be further identified. The basic idea for quantifying TR is to first establish the joint distribution between the soil moisture series of each month and the accumulated precipitation series under the corresponding PT. Then, using conditional probability formula (Eq. (5)), calculate the probability of soil moisture drought occurrence under different levels of precipitation deficits, and finally select the TR for drought propagation based on this probability. The specific procedures are as follows:

Firstly, the probability of soil moisture drought caused by different precipitation intervals under the PT accumulation scale is calculated with following equation:

$$
\begin{aligned}
P_j &= P\left(SM_j < sm \mid pr-1 < Pr_{j\,pt} < pr\right) \\
&= \frac{P\left(SM_j < sm, pr-1 < Pr_{j\,pt} < pr\right)}{P\left(pr-1 < Pr_{j\,pt} < pr\right)} \\
&= \frac{P\left(SM_j < sm, Pr_{j\,pt} < pr\right) - P\left(SM_j < sm, Pr_{j\,pt} < pr-1\right)}{P\left(Pr_{j\,pt} < pr\right) - P\left(Pr_{j\,pt} < pr-1\right)} \\
&= \frac{C\left(F_{SM_j}(sm), F_{Pr_{j\,pt}}(pr)\right) - C\left(F_{SM_j}(sm), F_{Pr_{j\,pt}}(pr-1)\right)}{F_{Pr_{j\,pt}}(pr) - F_{Pr_{j\,pt}}(pr-1)}
\end{aligned}
\tag{5}
$$

where *pt* is the drought PT in month *j*, $Pr_{j\,pt}$ represents the total amount of precipitation within the duration range of PT. $SM_j$ represents the status of soil moisture in month *j*, *sm* refers to the soil moisture content corresponding to the occurrence of drought at the *ds* grade. *pr* is a looping variable whose initial value represents the total precipitation amount (accumulated within the PT time range) corresponding to the occurrence of meteorological drought at the *ds* grade. $P_j$ refers to the probability of triggering soil moisture drought under the state range of precipitation total within [*pr*-1, *pr*].

Next, the precipitation interval [pr-1, pr] will be iteratively reduced by a step of 1mm, and Eq.5 will be used to calculate the probability values of soil moisture drought caused under different precipitation intervals. When the probability value exceeds the preset threshold of 0.8 (to ensure that TR has higher reliability, we set a probability threshold higher than that of PT), the iteration is stopped. At this point, TR is equal to the difference between the multi-year average precipitation in the PT time range and the pr value at the end of the iteration ($TR = \overline{Pr} - pr$, where $\overline{Pr}$ is the multi-year average precipitation). In other words, TR represents the total precipitation

deficit relative to normal state that is required to trigger soil moisture drought, and its unit is millimeters.

### *3.3 Exploring drought propagation dynamics and possible drivers*

In order to identify the dynamic trend of the propagation characteristics in the changing environments, we segmented the original data using a sliding window with a length of 31 years, and then calculated each window independently by the method described in Section 3.2 to determine how drought PT and TR have changed over recent decades. To test the significance of the trend, the Mann-Kendall trend test method (MK) with a significance level of 0.05 was used (Burn and Hag Elnur, 2002).

This study used Random Forest model to evaluate the importance of different predictors for identifying possible drivers of the trend in propagation characteristics. The Random Forest model is one of machine learning algorithms, which was first proposed by Breiman (2001) and has been widely used to solve classification and regression problems (Giri et al., 2023; Rosecrans et al., 2022). The model is essentially a classifier with multiple decision trees, its operation step is to first use the Bootstrap resampling method to randomly extract multiple samples from the original data, then train and fit each Bootstrap sample to build a regression tree, and finally the final result is obtained by averaging with the prediction results of all regression trees (Jing et al., 2020; Xie et al., 2021). It is a nonlinear modeling tool that has a reliable result for solving multivariate prediction problems and has a good tolerance to outliers and noise (Chagas et al., 2016; Guo et al., 2015; Zhang et al., 2017). In this study, we

established a Random Forest model consisting of 500 regression trees. The CART method was used to split the decision tree, and the minimum terminal node size was defined as 5. Then, we used the permutation importance method to rank the importance of each influencing variable. The specific approach is to randomly shuffle the normal time sequence of the detection variables, and re-inputting the broken variables into the model for calculation. The importance of the variables is evaluated based on the degree of decrease in model prediction accuracy, with greater decreases indicating a larger impact of the variable on the dependent variable (Pham and Brabyn, 2017). We use the Random Forest model to rank the importance of the main driving factors (such as Aridity index (AI), precipitation change (P), Vapor pressure deficit (VPD) and Normalized difference vegetation index (NDVI)), and to identify the dominant factors that affect the drought propagation characteristics. For more details about the Random Forest algorithm can refer to the literature (Huang et al., 2022; Xie et al., 2021). In addition, the introduction and calculation method of AI and VPD are shown in Appendix S1.

# 4 Results

## *4.1 Dependence of soil moisture on precipitation in growing season*

Before establishing the joint distribution between soil moisture and precipitation in the study area, the correlation of soil moisture and precipitation at different cumulative scales was analyzed. As shown in Fig. 4 (a), the maximum correlation coefficient between SPI and SSMI series was selected to draw the spatial-temporal

distribution diagram. In general, the soil moisture and precipitation showed a positive correlation in each month of the growing season. From the time perspective, the correlation in the early growing season (i.e., May to June) is slightly lower than in the middle and late periods (i.e., July to September). This difference is probably associated with the snow cover and frozen soil melting that weaken the link between soil water and precipitation during the early growing season (Chen et al., 2022; Wang et al., 2015). From the perspective of spatial distribution, the correlation is relatively high in the western part of the NEC, while lower in the central region. For the western part, the lack of rains making a strong link between soil moisture and precipitation. In contrast, the central region occupies mostly low-lying alluvial plains, where farmland, wetlands, and marshes are widely spread. The soil moisture content is thus higher than that in other regions, with a relatively weak natural connection to precipitation.

In addition, the optimal response time of the soil moisture to the precipitation (i.e., SPI accumulation time corresponding to the maximum correlation coefficient) is shown in Fig. 4 (b). In the early stage of the growing season, the response time is longer and gradually shortens as the month progresses. During the early growing season when temperature is generally low, evaporation and dissipation capacity of soil water are limited, and early snowfall and frozen soil dissolution can further replenish soil moisture. As a result, soil moisture is relatively weakly dependent on precipitation and responds slowly to the possible precipitation deficits. At the later stage of the growing season, however, with the increase in temperature and evapotranspiration, the connection between soil moisture and precipitation is strengthened, which reduces the

response time. In general, soil moisture in the NEC depends heavily on precipitation in the growing season, which is the precondition to establishing the joint distribution of soil moisture and precipitation and calculating the drought PT.

---

Place **Fig. 4** here.

**Fig. 4.** Natural dependence between soil moisture and precipitation, (a) spatial distribution of the maximum Pearson correlation coefficients between the monthly SSMI and SPI at contrasting timescales varying from 1 to 36 tendays for the period 1962–2014, (b) optimal response time of the soil moisture to the precipitation series.

---

### *4.2 Propagation time from meteorological to soil moisture drought*

Fig. 5 shows the spatiotemporal distribution of drought PT in the study area, and Fig. 8 (a) summaries the spatial average of drought PT for grids under different drought grades in each month of the growing season.

In terms of time, the PT in the early growing season (i.e., May to June) is relatively long (generally exceeding 200 days), while it shortens in the middle and late growing seasons (i.e., July to September) (Fig. 8 (a)). In most regions of the study area, the PT in July and August is typically less than 30 days, the shortest level of the entire growing season, while the PT in September is slightly longer roughly from 40 to 100 days (Fig. 5). As seen from space, the PT is longer in the central plain, western plateau area and northern high-latitude coniferous forest areas than it is elsewhere. It

is further obvious that the PT required progressively increases as soil moisture droughts worsen (Fig. 8 (a)). The blank part in Fig. 5 indicates that the probability of soil moisture drought caused by meteorological drought does not exceed the predefined probability threshold (i.e., 0.6 in the case). Note that with the drought severity increases, more grids fail to meet the requirement of probability, especially in the central region.

---

Place **Fig. 5** here.

**Fig. 5.** PT from meteorological drought to soil moisture drought under different grades in growing season, from top to bottom, each row in the figure represents the PT required to cause soil moisture drought with over mild, moderate and severe grades.

---

The above temporal and spatial patterns of the PT are largely related to the water and heat conditions during the growing season, as well as the topography and underlying surface conditions. When it comes to a mild soil moisture drought, for example, in the early growing season (i.e., May to June), the temperature is relatively low (Fig. 6(a)) and the evaporation is also weak, so the soil water cannot dissipate as readily. In addition, plant leaves are not fully developed in the early growing season (Fig. 6(d)), which reduces the demand for soil water and vapor that can pass through stomata (Hao et al., 2021). The relatively high latitude of NEC and the long cold winter that resulted in the large amount of snow and frozen soil melting in the western

and northern regions can also contribute to soil moisture (Peng et al., 2016; Wang et al., 2019; Xu et al., 2022). In light of the above reasons, soil moisture loss can be slower during early growing season when precipitation is lacking, and soil water can be replenished to some extent, resulting in a relatively difficult propagation of signals from the meteorological drought to the soil moisture and thus relatively long PT. However, even though the precipitation of soil replenishment increased in the summer (see Fig. 6(b)), as the temperature and solar radiation reached their highest level of the whole growing season, soil water evaporation accelerated. Meanwhile, the plant leaves have been fully developed, thus the water vapor dissipated by the vegetation has also enhanced (Zhang and Zhang, 2019). Therefore, when the meteorological drought comes, the water stored in the soil will be quickly dissipated through the soil surface and foliar under the promotion of high temperature, causing the soil moisture drought to occur and the shortest PT in July and August. In September, the dissipation rate of soil moisture decreased along with the decrease in temperature and vegetation greenness, prolonging the drought PT slightly.

From the perspective of spatial distribution, the central, northern, and western regions of the study area have longer PT than other regions (especially in July), which may be explained by the terrain and underlying surface conditions in the region. The area with a long PT in the central region of the study area is mainly located in the Songnen Plain, which is mainly formed by erosion and alluviation of the Songhua River and Nenjiang River. This region has relatively low terrain, a dense river network, and a high soil moisture content (Fig. 6(c)), which makes the connection

505 between soil moisture and precipitation relatively weak (it can be seen from the low
506 correlation between soil moisture and precipitation in the central region of Fig. 4 (a)).
507 Consequently, meteorological droughts usually take a longer PT to cause soil moisture
508 droughts in the region. Western and northern parts of the NEC, on the other hand, are
509 located in the Inner Mongolia Plateau and the Greater Khingan Mountains,
510 respectively. Both have high altitudes, especially in the western region, where the
511 average altitude exceeds 2,000 m (Fig. 2(a)). The resulting low temperatures may
512 weaken the relationship between soil moisture drought and meteorological drought.
513 Further, the northern region is dominated by coniferous forest (Fig. 2 (c)). As
514 compared to broad-leaved forests distributed in other mountains in the study area,
515 coniferous forests have smaller leaf areas and weaker transpiration (Ouyang et al.,
516 2021), and their soil water demands are also lower than broad-leaved forests. As a
517 result of above factors, soil moisture consumption rates are relatively low when
518 meteorological drought occurs, which may explain the longer PT in both regions.
519 Furthermore, when the soil moisture drought grades grow, meteorological droughts
520 often require accumulating for a longer period to cause higher grades. In the
521 meanwhile, the grid that is capable of reaching the trigger probability will also
522 decrease, which is more evident in areas with a weak dependence between soil
523 moisture and precipitation (see Fig. 4 (a) and Fig. 5).
524 ---

525 Place **Fig. 6** here.

526 **Fig. 6.** Meteorological and underlying surface conditions in the study area, (a)

temperature distribution in each month of the growing season, (b) precipitation distribution in each month of the growing season, (c) soil moisture distribution map in each month of the growing season, and (d) spatial and temporal distribution of NDVI index in the study area.

---

Overall, the drought PT in the vast areas of the NEC is usually the shortest in July and August. In this case, soil moisture drought caused by meteorological drought is often less than one month, which leaves little time for people to prepare and respond. It is therefore extremely unfavorable for early warning of droughts, which should be of great concern to water resources managers.

### *4.3 The trigger threshold of meteorological drought driving soil moisture drought*

Fig. 7 illustrates the spatial distribution of TR required to trigger different grades of soil moisture drought, and Fig. 8 (b) shows the regional average of the TR to trigger different grades of soil moisture drought during the growing season. In the figures, it is clear that TR distribution has remained relatively constant over time, while it is lower in the western region than in the central and eastern regions (generally below 80mm), which is mainly because of the relatively low precipitation in the western region (Fig. 2(b)). In addition, as soil moisture drought intensify, the TR required to trigger soil moisture drought also increases. For mild soil moisture droughts, a precipitation deficit around 80mm is needed, while moderate and severe droughts require a TR exceeding 120 and 140mm, respectively (Fig. 8 (b)). Furthermore, the

548 TR has different temporal pattern compared to PT, and it does not show an obvious
549 downward trend in the middle and late growing season (Fig. 8), in which case the
550 temporal pattern of precipitation plays a large role. The precipitation in NEC is
551 mainly concentrated in the middle and late growing seasons (summer) (Fig. 6(b)).
552 Despite the short PT, due to the large amount of precipitation, a higher TR can be
553 accumulated rapidly. However, in the early growth season, the precipitation
554 accumulation range when calculating TR is mainly in spring and winter. In spite of
555 the long PT in this case, the low precipitation limits the total amount of precipitation
556 accumulated, so there is no significant difference between TR in the early and late
557 growing seasons.

558 Note that the TR was calculated by directly analyzing precipitation and soil
559 moisture without standardized processing, which made the soil moisture drought
560 states of the regional grid reflected by the TR cannot be directly compared in space. It
561 is possible, however, to combine TR with the drought PT to provide important
562 reference information for the regional drought warning and prevention. Taking a
563 specific month of the growing season as an example. First, the time range for
564 detecting precipitation status can be determined in advance according to the drought
565 PT of that month, and then the deficit between the current precipitation and the
566 historical average within this cumulative scale can be calculated, which can be further
567 compared with the TR in that month. If the actual precipitation deficits that exceed the
568 drought TR, indicate that a soil moisture drought is likely to occur in that month. The
569 water gap needed to block the propagation of drought signal from meteorological to

570 soil moisture drought can be also obtained by subtracting actual precipitation deficits
571 from TR. By comparing the water gap with the current available water, the severity of
572 soil moisture drought and economic losses can be probably estimated in advance.
573 Therefore, according to the above methods, using the PT and TR under different
574 drought grades, an early warning system for soil moisture drought in each month of
575 the growing season can be developed to prevent and control drought precisely.
576 Furthermore, more drought information can be obtained by adjusting the extraction
577 probability thresholds of PT and TR (details will be elaborated in the Discussion
578 section).
579 ----------

580 Place **Fig. 7** here.

581 **Fig. 7.** The distribution of TR from meteorological drought to different grades of soil
582 moisture drought in the growing season.
583 ----------

584

585 ----------

586 Place **Fig. 8** here.

587 **Fig. 8.** Average distribution of PT and TR for different grades of soil moisture drought
588 in the growing season.
589 ----------

590 ***4.4 The dynamics of drought propagation characteristics in a changing***
591 ***environment***

592 In recent studies, NEC has been presented a significant warming trend (Zhang et al.,

2022). A major focus of the study is how the propagation from meteorological drought to soil moisture drought will be affected by the changing environment, especially in terms of the PT. In this study, 31-year sliding windows were used to segment the original data, and the PT under each window was calculated to obtain the sequence of dynamic changes in the PT, then the Mann-Kendall method was used to test its significance.

Fig. 9 shows the dynamic change trend of the drought PT in recent decades. A darker red in the figure indicates a more pronounced shortening of PT, while blue represents the opposite (grids with a dot indicate a significant trend ($\alpha$=0.05)). During the early growing season (i.e., May and June), the drought PT showed a significant prolonging trend in the whole study area except for a few grids in the western region. As of July, however, the overall prolonging trend of PT started to weaken, and the central and eastern regions even showed a significant shortening trend. During the late growth season (i.e., August and September), the overall dynamics of PT shifted from an early prolonging trend to a significant shortening trend, especially in the central and western regions.

---

Place **Fig. 9** here.

**Fig. 9.** Dynamic trend of drought PT in recent decades under the changing environment background.

---

Several factors affect the propagation process of drought signals from the atmosphere

to the soil moisture system along the hydrological cycle, but they can be divided into two basic categories according to the cycle process of soil moisture: source and expenditure. Therefore, precipitation (P), the main source of soil water, together with the Aridity index (AI) and vapor pressure deficit (VPD), which affect soil moisture consumption, were selected as the potential drivers of the changing PT. Their importance was evaluated using a Random Forest model, the importance of different influencing factors to PT in each month of the growing season was evaluated. Fig. 10 shows the spatial distribution of the two factors that have the greatest impacts on the PT. Obviously, PT in most regions in May is mainly affected by VPD and precipitation, whereas in June, precipitation dominates the north of the study area with VPD dominating the west and southeast. In comparison, as of July, the area with significantly shortened PT was mainly affected by VPD, while the area with a prolonging trend is mainly affected by precipitation in the southeast region. In August and September, the area where the PT is shortened was primarily affected by the VPD and AI.

In early growing season (May and June), drought PT is characterized by a prolonged trend. The above analysis indicates that VPD might be an important factor, but could be also associated with the rising trend in temperature that makes the VPD rise in the study area (Fig. S1(a) and S1(d)). As a result of the high latitude of NEC, the soil surface still stores more snow and frozen soil in the early growing season (Chen et al., 2022; Wang et al., 2015). The residual snow and frozen soil in winter and spring supplement soil water can more rapidly in a warming climate, which alleviates

637 the soil moisture drought (Wang et al., 2019). Furthermore, precipitation in most areas
638 also increased (Fig. S1(b)), which further supplemented soil moisture to reduce the
639 impact of drought. Therefore, although the VPD shows an upward trend in the early
640 growing season, the PT is prolonged due to snow melting and increased precipitation.
641 As of July, the significant shortening trend of PT in the central and eastern regions of
642 the study area was mainly due to an increase in VPD. This is because the snow and
643 frozen soil have dissolved at that time, and the higher VPD caused by the rising
644 temperature will increase the water demand of the atmosphere (Fig. S1(d)), which will
645 directly accelerate the actual evaporation consumption from the soil. In the southeast
646 region, the prolonging of PT may be due to increased precipitation, which replenishes
647 soil moisture and slows down the formation process of soil moisture drought.
648 Following the late growing season, the drought PT in most regions was significantly
649 shortened, mainly due to the changing of VPD and AI. As can be seen from Fig. S1(a),
650 the temperature of the whole region in the study area showed a significant rise in the
651 late growing season, resulting in an increase in VPD and potential evapotranspiration
652 (Fig. S1(d)). When the meteorological drought occurs, therefore, soil moisture will
653 dissipate more rapidly in evapotranspiration triggering quick soil moisture drought. In
654 addition, precipitation in the late growing season also shows a downward trend
655 throughout most of the study area (Fig. S1(b)), leading to a reduction of soil water
656 supplement and AI index, a drying trend in the regional climate, and eventually
657 accelerated drought propagation. Besides, the slight prolongation of drought PT in the
658 southeast of the study area may be related to the local increased precipitation.

---

Place **Fig. 10** here.

**Fig. 10.** The dominant factors of drought PT in each month of the growing season, (a) and (b) are the first and second important factors respectively.

---

It should be noted that the PT in the central and western regions is initially short in the late growing season. In this case, the shortened PT will make the reserved warning time become tenser, which will further aggravate the drought resistance challenge during the period. In addition to precipitation, VPD, and AI, vegetation also has a significant indirect impact on the trend in drought propagation, which will be discussed in detail in Section 5.1.

Furthermore, based on the PT under each sliding window, we further calculated the change sequence of TR, and analyzed its dynamic trend likewise using the Mann-Kendall method. As shown in Fig. 11, the change of TR is generally consistent with that of PT. Early growing season (i.e., May and June), drought TR has a significant prolonging trend, but by the middle and late growing season (i.e., from July to September), the drought TR begins to decline, especially in the central and western regions. The drought TR trend is largely affected by the change of drought PT. For example, the shortening of drought PT will shorten the precipitation accumulation scale, which will reduce drought TR, and vice versa in areas where drought PT is prolonged. Late in the growing season, both PT and TR were declining in the vast central and western regions, which means that when meteorological drought strikes, it

will take less time and lower precipitation deficit to trigger soil moisture drought. This case will lead to a greater risk of propagation between droughts, invalidating drought control and prevention efforts, and probably further deteriorating drought impacts.

---

Place **Fig. 11** here.

**Fig. 11.** Dynamic trend of drought TR in recent decades.

---

# 5 Discussion

## *5.1 The driving force analysis of drought propagation characteristic dynamics*

Previous studies have shown that warming plays an important role in the hydrological cycle, as the rise of temperature may aggravate the loss of water and lead to regional dryness and droughts (Trenberth et al., 2014).The significant warming in NEC leads to rise in VPD in the late growth season, thereby increasing the demand for water in the atmosphere, thus promoting the evaporation consumption of soil moisture (Li et al., 2020; Zhang et al., 2022; Zhou et al., 2020). Warming is also expected to increase potential evapotranspiration, together with the decreasing precipitation in the late growing season, resulting in a decline in the AI index and regional climate showing a drying trend. The above factors will significantly promote the actual evaporation of soil water and accelerate soil moisture drought, and

shortening PT in the late growth season.

In addition to precipitation, VPD and AI, vegetation also plays a critical role in the propagation of drought signals. Being the medium for water and energy exchange between soil and atmosphere systems, vegetation has significant impacts on regional water cycle and drought evolution (Gao et al., 2018; Huang et al., 2018). On the one hand, the sustained increase of vegetation coverage can increase soil water consumption in a certain area, which may exceed the water resource carrying capacity of the area, causing a decrease in soil water and making it more prone to soil moisture drought (Lian et al., 2020; Zhang et al., 2021). On the other hand, with the increase of vegetation greenness, when facing meteorological drought, as the VPD rises, soil water can evaporate quickly into the atmosphere through the stomata of vegetation leaves (Jiao et al., 2021), accelerating the rate of soil moisture consumption and ultimately shortening the propagation time from meteorological drought to soil moisture drought. Previous studies have also found that vegetation greening increases soil water loss by transpiration from an expanded leaf area (Chen et al., 2019; Zeng et al., 2018), and exacerbates the risk of regional drought (especially in arid and semiarid areas) (Deng et al., 2020; Zhang et al., 2022). In this study, the NDVI index was used to analyze the dynamic changes in the vegetation cover in NEC since 1982. It was found that the vegetation cover in the study area increased significantly in the late growing season, while in the early period, most of the areas mainly showed a downward trend (Fig. 12). NDVI series and hydrometeorological factors (P, VPD and AI) were introduced into the Random Forest model by using 19 sliding windows to

724 further quantify the impact of different factors on drought PT. Fig. S5 shows the
725 spatial distribution of two factors that have the most significant impact on the drought
726 PT. It can be seen that the vegetation cover change in some regions even exceeds the
727 direct impact of hydrometeorological factors on drought propagation. With the
728 vegetation greening in the late growing season, when meteorological drought occurs,
729 soil water may be rapidly evaporated and consumed through vegetation channels,
730 which accelerates the propagation process of drought signals in the atmosphere and
731 soil moisture. After normalizing the influences of various factors on drought
732 propagation processes, we found that the relative importance of NDVI could reach
733 more than 20% of the total importance (Fig.13), and the change of vegetation cover
734 had a significant impact on drought propagation. In addition, we found that vegetation
735 also has an impact on the drought propagation in the early growing season (May to
736 June), which is mainly related to the decline of large area vegetation cover in the
737 central and eastern regions (Fig. 12). With the decline of vegetation cover, its demand
738 for water decreased, indirectly alleviating soil moisture consumption and prolonging
739 the drought PT during this period. However, the increase of vegetation cover in the
740 western edge regions in the early growing season may accelerate the consumption of
741 soil water and shorten the drought PT in this area.

742 ---

743 Place **Fig. 12** here.

744 **Fig. 12.** Dynamic trend of NDVI in growing season from 1982 to 2014.

745 ---

746

747 ----------

748 Place **Fig. 13** here.

749 **Fig. 13.** Relative contribution rate of different influencing factors to drought

750 propagation trend.

751 ----------

752 ***5.2 Sensitivity analysis of some important results regarding threshold and sliding***

753 ***window length set***

754 In this study, the dynamic change trend of drought PT and TR from 1962 to 2014

755 was evaluated by using a 31-years sliding window. In order to avoid the influence of

756 the length of the selected sliding window on the results, different lengths (i.e., 19, 23,

757 27, and 35 years) were used for verification respectively. The results show that the

758 dynamic trend of PT and TR is basically independent of the length of the sliding

759 window, and the change trend under different windows is largely consistent (Fig. S3

760 and S4), which indicates the robustness of the results.

761 When determining the drought PT and TR, we set different extraction probability

762 thresholds. Fig. S2 shows the conditional probability matrix of soil moisture drought

763 in the calculation of drought PT with 15 randomly selected grids. The vertical

764 coordinate in the figure represents the time cumulative scale of SPI, and the horizontal

765 coordinate represents each month of the 15 grids in the growing season. It can be seen

766 from the figure that it often requires a longer time accumulation in the early growing

767 season to make the probability of soil moisture drought to reach a higher level, while

768 the time required in the late growth season is relatively short. The probability value of
769 each month increases continuously with the rising of cumulative time, and gradually
770 remains unchanged after reaching a higher level. When extracting the drought PT, we
771 did not choose the meteorological drought accumulation scale corresponding to the
772 highest probability of soil moisture drought, but instead took 0.6 as the probability
773 threshold. The reason for this is that the PT extracted under the highest probability is
774 generally extensively long, and the cumulative time before the maximum probability
775 is also prone to causing soil moisture drought (Li et al., 2022). We therefore selected a
776 medium probability (0.6) to extract the drought PT so as not to ignore the short
777 drought PT. In addition, when determining the TR, we set a higher probability
778 threshold (0.8) than the extraction of PT to further ensure the credibility of causing
779 soil moisture drought.

780 In addition, in the practical drought warning operation, the probability threshold for
781 extracting propagation time can be flexibly adjusted to obtain different lengths of PT,
782 which can be combined with the TR to grasp the development status of drought and
783 respond in a timely manner. Taking the drought warning of a certain month as an
784 example, first collect precipitation data from the preceding month and obtain a longer
785 PT by increasing the probability threshold (e.g., 0.65, 0.7, 0.8). PT. Next, calculate the
786 total precipitation within the time range of the PT, subtract it from the long-term
787 average to obtain the actual precipitation deficit. Finally, compare the precipitation
788 deficit with the drought TR of that month. If the precipitation deficit exceeds TR, it
789 indicates a high possibility of triggering soil moisture drought. At this time, water

790 resource managers should take timely measures to block the propagation chain of
791 drought by reasonable allocation of water resources. On the contrary, if the
792 precipitation deficit does not exceed TR, it indicates a lower possibility of soil
793 moisture drought occurring at this time. The probability threshold of PT can then be
794 lowered to obtain a shorter drought PT, and the precipitation deficit within the new
795 time accumulation range should be checked again to see if it exceeds the TR value.
796 Therefore, by repeatedly adjusting and testing the possibility of drought occurrence,
797 we can timely understand the development status of drought and try to avoid biases
798 and misjudgments caused by a single judgment as much as possible. Based on the
799 drought early warning system described above, reliable PT and TR can be used to
800 obtain key drought-resistant information. For example, by subtracting TR from the
801 actual precipitation deficit, we can determine the necessary water quantity for
802 alleviating soil moisture drought, and compare this water deficit with the currently
803 available water resources to estimate the potential range of drought impact and
804 possible economic losses in advance.

805 ***5.3 Comparison analysis between some findings of this study and previous studies***

806 Drought PT is an important characteristic of drought signal propagation between
807 atmospheric and soil moisture system (Zhang et al., 2021). Moreover, accurate PT is a
808 prerequisite to estimating the TR of soil moisture drought. In this study, using the
809 Bayesian causal analysis framework, the conditional probability of soil moisture
810 drought was used to determine the PT. Compared to the traditional correlation
811 coefficient method, the conditional probability method can directly separate the

propagation signal from the dependency relationship between precipitation and soil moisture to avoid the interference from non-drought information (Dai et al., 2022; Wu et al., 2021). Additionally, the propagation process can be analyzed under different drought grades (Li et al., 2022; Zhu et al., 2021). This study, shows that the PT is long in the early growing season (spring and early summer), and relatively short in the middle and late growing period (summer and autumn), which is consistent with the seasonal distribution of drought PT in previous studies (Xu et al., 2021; Zhang et al., 2022). However, the PT in the early growing season (May and June) in NEC is longer than previous research findings, possibly associated with the geography of the region. The study area is located in the northernmost part of China. Compared with other regions in the same period, its higher latitude results in lower temperature and relatively weak evaporation capacity, and it has plenty of natural forest land, which can prolong the melting time of ice, snow, and frozen soil (Wang et al., 2015; Wang et al 2019). The solid water melted into the soil during the early growing season as the temperature increased, alleviating the soil moisture drought, slowing the propagation of drought, and making PT from meteorological to soil moisture drought over 270 days (Fig. 8(a)). In the same period, however, the PT in the Loess Plateau, located in the inland region of northwest China, generally does not exceed 6 months (Dai et al., 2022; Li et al., 2022). Furthermore, the drought PT and TR in most areas of NEC have shown a significant downward trend during the late growing season, which will exacerbate the risk of drought propagation, accelerate the formation of soil moisture droughts, and ultimately increase the possibility of ‘flash drought’ in these areas (Xu

et al., 2021; Zhu et al., 2021). The literature, revealed that the frequency, duration, and intensity of 'flash drought' in NEC increased from 1961 to 2016 (Zhang et al., 2022), which is agrees with our findings.

## 6 Conclusion

In this study, PT and TR of meteorological drought to the soil moisture drought with different drought grades were determined using the Copula functions and a Bayesian causal analysis framework. We also assessed the dynamic trend of drought propagation characteristics in recent decades under the warming and greening background and identified the possible driving factors on the drought propagation, the main conclusions of this study are as follows:

(1) In early growing season (i.e., May and June), the PT required to cause soil moisture drought is longer, with an average of more than 200 days. And after entering the middle and late growing season (i.e., from July to September), PT began to shorten, and the shortest PT in July and August was generally less than 30 days. The temporal and spatial distribution of drought PT is mainly related to the water and energy characteristics in each month of the growing season and the regional underlying surface conditions. In addition, with the aggravation of soil moisture drought, the PT required to cause soil moisture drought also increased.

(2) The distribution of TR in the NEC has remained relatively constant over time. Spatially, the TR in the western region of the study area is relatively low, generally below 80mm, while it is high in the central and eastern regions. This is

855 mainly related to the overall pattern of precipitation showing more in the east and
856 less in the west in the study area. Furthermore, the TR required to trigger soil
857 moisture drought also have an increasing trend with the increasing grades of
858 drought.

859 (3) Dynamic trend analysis of drought propagation characteristics indicates that the
860 drought PT in the early growing season (i.e., May and June) shows a prolonging
861 trend in most regions of the study area, which may be related to the accelerated
862 dissolution of snow cover and frozen soil and the decline of vegetation cover
863 during this period. However, in the late growing season (i.e., from July to
864 September), the situation began to reverse, the PT and TR showed a significant
865 downward trend in the central and western regions of the study area. And the
866 analysis found that the temperature showed a significant rising trend in the late
867 growing season, which driving the increase of VPD and the decrease of AI, and
868 the vegetation greening also played an important role in this period. These factors
869 together increased the rate of soil water consumption and accelerated the
870 propagation of drought signals.

871 It should be noted that in the late growing season, due to the dual impacts of
872 warming and vegetation greening, the risk of drought propagation is greatly increased,
873 resulting in both the PT and TR showed a significant downward trend in the central
874 and western regions of the NEC, which will make these regions faster and easier to
875 cause soil moisture drought after the meteorological drought occurs, and the response

time reserved for people will be shortened. Furthermore, the drought PT and TR can be used together to obtain important drought resistance information in advance. This method is relatively simple and can be used in other regions to help policy makers, water resources managers, and local stakeholders develop proactive drought mitigation, response, and preparation plans in a timely manner.

## Acknowledgements

This study was jointly funded by the Strategic Priority Research Program of the Chinese Academy of Sciences (grant number. XDA28060100), and the National Natural Science Foundation of China (grant number 52279026).

## References

Apurv, T., Sivapalan, M., Cai, X., 2017. Understanding the Role of Climate Characteristics in Drought Propagation. Water Resour. Res. 53, 9304–9329. https://doi.org/10.1002/2017WR021445

Barker, L.J., Hannaford, J., Chiverton, A., Svensson, C., 2016. From meteorological to hydrological drought using standardised indicators. Hydrol. Earth Syst. Sci. 20, 2483–2505. https://doi.org/10.5194/hess-20-2483-2016

Bevacqua, A.G., Chaffe, P.L.B., Chagas, V.B.P., AghaKouchak, A., 2021. Spatial and temporal patterns of propagation from meteorological to hydrological droughts in Brazil. J. Hydrol. 603, 126902. https://doi.org/10.1016/j.jhydrol.2021.126902

Bonan, G.B., 2008. Forests and climate change: Forcings, feedbacks, and the climate

benefits of forests. Science (80-. ). 320, 1444–1449. https://doi.org/10.1126/science.1155121

Burn, D.H., Hag Elnur, M.A., 2002. Detection of hydrologic trends and variability. J. Hydrol. 255, 107–122. https://doi.org/10.1016/S0022-1694(01)00514-5

Chagas, S., Junior, W.D.C., Bhering, S.B., Filho, B.C., 2016. Catena Spatial prediction of soil surface texture in a semiarid region using random forest and multiple linear regressions. Catena 139, 232–240. https://doi.org/10.1016/j.catena.2016.01.001

Chen, C., Park, T., Wang, X., Piao, S., Xu, B., Chaturvedi, R.K., Fuchs, R., Brovkin, V., Ciais, P., Fensholt, R., Tømmervik, H., Bala, G., Zhu, Z., Nemani, R.R., Myneni, R.B., 2019. China and India lead in greening of the world through land-use management. Nat. Sustain. 2, 122–129. https://doi.org/10.1038/s41893-019-0220-7

Chen, Tian, F., Su, Y., 2022. How did the late 1920s drought affect northern Chinese society? Weather Clim. Extrem. 36, 100451. https://doi.org/10.1016/j.wace.2022.100451

Chen, X., Li, X., Wang, G., Zheng, X., 2022. Faster velocity changes in the near-surface soil freeze state in croplands than in forests across northeast China from 1979 to 2020. J. Environ. Manage. 321, 116022. https://doi.org/10.1016/j.jenvman.2022.116022

Cheng, Y., Liu, L., Cheng, L., Fa, K., Liu, X., Huo, Z., Huang, G., 2022. A shift in the dominant role of atmospheric vapor pressure deficit and soil moisture on vegetation greening in China. J. Hydrol. 615, 128680. https://doi.org/10.1016/j.jhydrol.2022.128680

Choudhury, A., Dutta, D., Bera, D., Kundu, A., 2021. Regional variation of drought parameters and long-term trends over India using standardized precipitation evapotranspiration index. J. Environ. Manage. 296, 113056. https://doi.org/10.1016/j.jenvman.2021.113056

Dai, M., Huang, S., Huang, Q., Zheng, X., Su, X., Leng, G., Li, Z., Guo, Y., Fang, W., Liu, Y., 2022. Propagation characteristics and mechanism from meteorological to agricultural drought in various seasons. J. Hydrol. 610, 127897. https://doi.org/10.1016/j.jhydrol.2022.127897

Deng, Y., Wang, S., Bai, X., Luo, G., Wu, L., Chen, F., Wang, J., Li, C., Yang, Y., Hu, Z., Tian, S., Lu, Q., 2020. Vegetation greening intensified soil drying in some semi-arid and arid areas of the world. Agric. For. Meteorol. 292–293, 108103. https://doi.org/10.1016/j.agrformet.2020.108103

Fang, W., Huang, S., Huang, Q., Huang, G., Wang, H., Leng, G., Wang, L., Guo, Y., 2019. Probabilistic assessment of remote sensing-based terrestrial vegetation vulnerability to drought stress of the Loess Plateau in China. Remote Sens. Environ. 232, 111290. https://doi.org/10.1016/j.rse.2019.111290

Gao, S., Liu, R., Zhou, T., Fang, W., Yi, C., Lu, R., Zhao, X., Luo, H., 2018.

937 Dynamic responses of tree-ring growth to multiple dimensions of drought. Glob.
938 Chang. Biol. 24, 5380–5390. https://doi.org/10.1111/gcb.14367

939 Ge, X., Zhu, J., Lu, D., Wu, D., Yu, F., Wei, X., 2022. Effects of canopy composition
940 on snow depth and below-the-snow temperature regimes in the temperate
941 secondary forest ecosystem, Northeast China. Agric. For. Meteorol. 313, 108744.
942 https://doi.org/10.1016/j.agrformet.2021.108744

943 Giri, S., Kang, Y., Macdonald, K., Tippett, M., Qiu, Z., Lathrop, R.G., Obropta, C.C.,
944 2023. Science of the Total Environment Revealing the sources of arsenic in
945 private well water using Random Forest Classi fi cation and Regression. Sci.
946 Total Environ. 857, 159360. https://doi.org/10.1016/j.scitotenv.2022.159360

947 Guo, E., Liu, X., Zhang, J., Wang, Y., Wang, C., Wang, R., Li, D., 2017. Assessing
948 spatiotemporal variation of drought and its impact on maize yield in Northeast
949 China. J. Hydrol. 553, 231–247. https://doi.org/10.1016/j.jhydrol.2017.07.060

950 Guo, P., Li, M., Luo, W., Tang, Q., Liu, Z., Lin, Z., 2015. Geoderma Digital mapping
951 of soil organic matter for rubber plantation at regional scale : An application of
952 random forest plus residuals kriging approach. Geoderma 237–238, 49–59.
953 https://doi.org/10.1016/j.geoderma.2014.08.009

954 Guo, W., Huang, S., Huang, Q., Leng, G., Mu, Z., Han, Z., Wei, X., She, D., Wang,
955 H., Wang, Z., Peng, J., 2023. Drought trigger thresholds for different levels of
956 vegetation loss in China and their dynamics. Agric. For. Meteorol. 331, 109349.
957 https://doi.org/10.1016/j.agrformet.2023.109349

Guo, Y., Huang, S., Huang, Q., Leng, G., Fang, W., Wang, L., Wang, H., 2020. Propagation thresholds of meteorological drought for triggering hydrological drought at various levels. Sci. Total Environ. 712, 136502. https://doi.org/10.1016/j.scitotenv.2020.136502

Han, Z., Huang, Q., Huang, S., Leng, G., Bai, Q., Liang, H., Wang, L., Zhao, J., Fang, W., 2021a. Spatial-temporal dynamics of agricultural drought in the Loess Plateau under a changing environment: Characteristics and potential influencing factors. Agric. Water Manag. 244, 106540. https://doi.org/10.1016/j.agwat.2020.106540

Han, Z., Huang, S., Huang, Q., Leng, G., Liu, Y., Bai, Q., He, P., Liang, H., Shi, W., 2021b. GRACE-based high-resolution propagation threshold from meteorological to groundwater drought. Agric. For. Meteorol. 307, 108476. https://doi.org/10.1016/j.agrformet.2021.108476

Hao, Y., Fu, Y.H., Sifang, F., 2021. Probabilistic assessments of the impacts of compound dry and hot events on global vegetation during growing seasons Probabilistic assessments of the impacts of compound dry and hot events on global vegetation during growing seasons. https://doi.org/10.1088/1748-9326/ac1015

Huang, K., Xia, J., Wang, Y., Ahlström, A., Chen, J., Cook, R.B., Cui, E., Fang, Y., Fisher, J.B., Huntzinger, D.N., Li, Z., Michalak, A.M., Qiao, Y., Schaefer, K., Schwalm, C., Wang, J., Wei, Y., Xu, X., Yan, L., Bian, C., Luo, Y., 2018.

Enhanced peak growth of global vegetation and its key mechanisms. Nat. Ecol. Evol. 2, 1897–1905. https://doi.org/10.1038/s41559-018-0714-0

Huang, M., Wang, Q., Jing, R., Lou, W., Hong, Y., Wang, L., 2022. Journal of Wind Engineering & Industrial Aerodynamics Tropical cyclone full track simulation in the western North Pacific based on random forests. J. Wind Eng. Ind. Aerodyn. 228, 105119. https://doi.org/10.1016/j.jweia.2022.105119

Huang, S., Li, P., Huang, Q., Leng, G., Hou, B., Ma, L., 2017. The propagation from meteorological to hydrological drought and its potential influence factors. J. Hydrol. 547, 184–195. https://doi.org/10.1016/j.jhydrol.2017.01.041

Jiao, W., Wang, L., Smith, W.K., Chang, Q., Wang, H., D'Odorico, P., 2021. Observed increasing water constraint on vegetation growth over the last three decades. Nat. Commun. 12, 1–9. https://doi.org/10.1038/s41467-021-24016-9

Jing, W., Zhang, P., Zhao, X., Yang, Y., Jiang, H., 2020. Extending GRACE terrestrial water storage anomalies by combining the random forest regression and a spatially moving window structure. J. Hydrol. 590, 125239. https://doi.org/10.1016/j.jhydrol.2020.125239

Kalisa, W., Zhang, J., Igbawua, T., Ujoh, F., Ebohon, O.J., Namugize, J.N., Yao, F., 2020. Spatio-temporal analysis of drought and return periods over the East African region using Standardized Precipitation Index from 1920 to 2016. Agric. Water Manag. 237, 106195. https://doi.org/10.1016/j.agwat.2020.106195

Konapala, G., Mishra, A., 2020. Quantifying Climate and Catchment Control on Hydrological Drought in the Continental United States. Water Resour. Res. 56, 1–25. https://doi.org/10.1029/2018WR024620

Kumar, R., Musuuza, J.L., Van Loon, A.F., Teuling, A.J., Barthel, R., Ten Broek, J., Mai, J., Samaniego, L., Attinger, S., 2016. Multiscale evaluation of the Standardized Precipitation Index as a groundwater drought indicator. Hydrol. Earth Syst. Sci. 20, 1117–1131. https://doi.org/10.5194/hess-20-1117-2016

Li, K., Tong, Z., Liu, X., Zhang, J., Tong, S., 2020. Quantitative assessment and driving force analysis of vegetation drought risk to climate change:Methodology and application in Northeast China. Agric. For. Meteorol. 282–283. https://doi.org/10.1016/j.agrformet.2019.107865

Li, P., Huang, Q., Huang, S., Leng, G., Peng, J., Wang, H., Zheng, X., Li, Y., Fang, W., 2022. Various maize yield losses and their dynamics triggered by drought thresholds based on Copula-Bayesian conditional probabilities. Agric. Water Manag. 261, 107391. https://doi.org/10.1016/j.agwat.2021.107391

Li, Y., Huang, S., Wang, H., Zheng, X., Huang, Q., Deng, M., Peng, J., 2022. High-resolution propagation time from meteorological to agricultural drought at multiple levels and spatiotemporal scales. Agric. Water Manag. 262, 107428. https://doi.org/10.1016/j.agwat.2021.107428

Li, Y., Piao, S., Li, L.Z.X., Chen, A., Wang, X., Ciais, P., Huang, L., Lian, X., Peng, S., Zeng, Z., Wang, K., Zhou, L., 2018. Divergent hydrological response to

1020 large-scale afforestation and vegetation greening in China. Sci. Adv. 4, 1–10.
1021 https://doi.org/10.1126/sciadv.aar4182

1022 Lian, X., Piao, S., Li, L.Z.X., Li, Y., Huntingford, C., Ciais, P., Cescatti, A., Janssens,
1023 I.A., Peñuelas, J., Buermann, W., Chen, A., Li, X., Myneni, R.B., Wang, X.,
1024 Wang, Y., Yang, Y., Zeng, Z., Zhang, Y., McVicar, T.R., 2020. Summer soil
1025 drying exacerbated by earlier spring greening of northern vegetation. Sci. Adv. 6,
1026 1–12. https://doi.org/10.1126/sciadv.aax0255

1027 López-Moreno, J.I., Vicente-Serrano, S.M., Zabalza, J., Beguería, S., Lorenzo-Lacruz,
1028 J., Azorin-Molina, C., Morán-Tejeda, E., 2013. Hydrological response to climate
1029 variability at different time scales: A study in the Ebro basin. J. Hydrol. 477,
1030 175–188. https://doi.org/10.1016/j.jhydrol.2012.11.028

1031 Mahecha, M.D., Bastos, A., Bohn, F.J., Eisenhauer, N., Feilhauer, H., Hartmann, H.,
1032 Hickler, T., Kalesse-Los, H., Migliavacca, M., Otto, F.E.L., Peng, J., Quaas, J.,
1033 Tegen, I., Weigelt, A., Wendisch, M., Wirth, C., 2022. Biodiversity loss and
1034 climate extremes — study the feedbacks. Nature 612, 30–32.
1035 https://doi.org/10.1038/d41586-022-04152-y

1036 McKee, T.B., Doesken, N.J., Kleist, J., 1993. Preoperative serum value of sialyl
1037 Lewis X predicts pathological nodal extension and survival in patients with
1038 surgically treated small cell lung cancer. J. Surg. Oncol. 105, 179–183.
1039 https://doi.org/10.1002/jso.23002

1040 Melsen, L.A., Guse, B., 2019. Hydrological Drought Simulations: How Climate and

1041 Model Structure Control Parameter Sensitivity. Water Resour. Res. 55, 10527–
1042 10547. https://doi.org/10.1029/2019WR025230

1043 Mishra, A.K., Singh, V.P., 2011. Drought modeling - A review. J. Hydrol.
1044 https://doi.org/10.1016/j.jhydrol.2011.03.049

1045 Mishra, A.K., Singh, V.P., 2010. A review of drought concepts. J. Hydrol. 391, 202–
1046 216. https://doi.org/10.1016/j.jhydrol.2010.07.012

1047 Ouyang, L., Wu, J., Zhao, P., Li, Y., Zhu, L., Ni, G., Rao, X., 2021. Consumption of
1048 precipitation by evapotranspiration indicates potential drought for broadleaved
1049 and coniferous plantations in hilly lands of South China. Agric. Water Manag.
1050 252, 106927. https://doi.org/10.1016/j.agwat.2021.106927

1051 Peng, J., Dadson, S., Hirpa, F., Dyer, E., Lees, T., Miralles, D.G., Vicente-Serrano,
1052 S.M., Funk, C., 2020. A pan-African high-resolution drought index dataset. Earth
1053 Syst. Sci. Data 12, 753–769. https://doi.org/10.5194/essd-12-753-2020

1054 Peng, J., Dadson, S., Leng, G., Duan, Z., Jagdhuber, T., Guo, W., Ludwig, R.,
1055 Jagdhuber, T., Guo, W., Ludwig, R., 2019. The impact of the Madden-Julian
1056 Oscillation on hydrological extremes. J. Hydrol.
1057 https://doi.org/10.1016/j.jhydrol.2019.01.055

1058 Peng, X., Frauenfeld, O.W., Cao, B., Wang, K., Wang, H., Su, H., Huang, Z., Yue, D.,
1059 Zhang, T., 2016. Response of changes in seasonal soil freeze/thaw state to
1060 climate change from 1950 to 2010 across china. J. Geophys. Res. Earth Surf. 121,

1984–2000. https://doi.org/10.1002/2016JF003876

Pham, L.T.H., Brabyn, L., 2017. Monitoring mangrove biomass change in Vietnam using SPOT images and an object-based approach combined with machine learning algorithms. ISPRS J. Photogramm. Remote Sens. 128, 86–97. https://doi.org/10.1016/j.isprsjprs.2017.03.013

Rosecrans, C.Z., Belitz, K., Ransom, K.M., Stackelberg, P.E., Mcmahon, P.B., 2022. Science of the Total Environment Predicting regional fl uoride concentrations at public and domestic supply depths in basin- fi ll aquifers of the western United States using a random forest model. Sci. Total Environ. 806, 150960. https://doi.org/10.1016/j.scitotenv.2021.150960

Seneviratne, S.I., Corti, T., Davin, E.L., Hirschi, M., Jaeger, E.B., Lehner, I., Orlowsky, B., Teuling, A.J., 2010. Investigating soil moisture-climate interactions in a changing climate: A review. Earth-Science Rev. 99, 125–161. https://doi.org/10.1016/j.earscirev.2010.02.004

Tijdeman, E., Blauhut, V., Stoelzle, M., Menzel, L., Stahl, K., 2022. Different drought types and the spatial variability in their hazard, impact, and propagation characteristics. Nat. Hazards Earth Syst. Sci. 22, 2099–2116. https://doi.org/10.5194/nhess-22-2099-2022

Trenberth, K.E., Dai, A., Van Der Schrier, G., Jones, P.D., Barichivich, J., Briffa, K.R., Sheffield, J., 2014. Global warming and changes in drought. Nat. Clim. Chang. 4, 17–22. https://doi.org/10.1038/nclimate2067

1082 Van Loon, A.F., 2015. Hydrological drought explained. Wiley Interdiscip. Rev. Water
1083 2, 359–392. https://doi.org/10.1002/WAT2.1085

1084 Vicente-Serrano, S.M., McVicar, T.R., Miralles, D.G., Yang, Y., Tomas-Burguera,
1085 M., 2020. Unraveling the influence of atmospheric evaporative demand on
1086 drought and its response to climate change. Wiley Interdiscip. Rev. Clim. Chang.
1087 11, 1–31. https://doi.org/10.1002/wcc.632

1088 Wan, W., Liu, Z., Li, J., Xu, J., Wu, H., Xu, Z., 2022. Spatiotemporal patterns of
1089 maize drought stress and their effects on biomass in the Northeast and North
1090 China Plain from 2000 to 2019. Agric. For. Meteorol. 315, 108821.
1091 https://doi.org/10.1016/j.agrformet.2022.108821

1092 Wang, K., Zhang, T., Zhong, X., 2015. Changes in the timing and duration of the
1093 near-surface soil freeze/thaw status from 1956 to 2006 across China. Cryosphere
1094 9, 1321–1331. https://doi.org/10.5194/tc-9-1321-2015

1095 Wang, W., Cui, W., Wang, X., Chen, X., 2016. Evaluation of GLDAS-1 and GLDAS-
1096 2 forcing data and noah model simulations over China at the monthly scale. J.
1097 Hydrometeorol. 17, 2815–2833. https://doi.org/10.1175/JHM-D-15-0191.1

1098 Wang, X., Chen, R., Liu, G., Yang, Y., Song, Y., Liu, J., Liu, Z., Han, C., Liu, X.,
1099 Guo, S., Wang, L., Zheng, Q., 2019. Spatial distributions and temporal variations
1100 of the near-surface soil freeze state across China under climate change. Glob.
1101 Planet. Change 172, 150–158. https://doi.org/10.1016/j.gloplacha.2018.09.016

1102 Wu, H., Su, X., Singh, V.P., Feng, K., Niu, J., 2021. Agricultural Drought Prediction
1103 Based on Conditional Distributions of Vine Copulas. Water Resour. Res. 57, 1–
1104 23. https://doi.org/10.1029/2021WR029562

1105 Wu, J., Chen, X., Yao, H., Liu, Z., Zhang, D., 2018. Hydrological Drought
1106 Instantaneous Propagation Speed Based on the Variable Motion Relationship of
1107 Speed-Time Process. Water Resour. Res. 54, 9549–9565.
1108 https://doi.org/10.1029/2018WR023120

1109 Wu, J., Chen, X., Yao, H., Zhang, D., 2021. Multi-timescale assessment of
1110 propagation thresholds from meteorological to hydrological drought. Sci. Total
1111 Environ. 765, 144232. https://doi.org/10.1016/j.scitotenv.2020.144232

1112 Xie, X., Wu, T., Zhu, M., Jiang, G., Xu, Y., Wang, X., Pu, L., 2021. Comparison of
1113 random forest and multiple linear regression models for estimation of soil
1114 extracellular enzyme activities in agricultural reclaimed coastal saline land. Ecol.
1115 Indic. 120, 106925. https://doi.org/10.1016/j.ecolind.2020.106925

1116 Xu, S., Fu, Q., Li, T., Meng, F., Liu, D., Hou, R., Li, M., Li, Q., 2022. Spatiotemporal
1117 characteristics of the soil freeze-thaw state and its variation under different land
1118 use types - A case study in Northeast China. Agric. For. Meteorol. 312.
1119 https://doi.org/10.1016/j.agrformet.2021.108737

1120 Xu, Y., Zhang, X., Hao, Z., Singh, V.P., Hao, F., 2021. Characterization of
1121 agricultural drought propagation over China based on bivariate probabilistic
1122 quantification. J. Hydrol. 598, 126194.

https://doi.org/10.1016/j.jhydrol.2021.126194

Yao, Y., Fu, B., Liu, Y., Li, Y., Wang, S., Zhan, T., Wang, Y., Gao, D., 2022. Evaluation of ecosystem resilience to drought based on drought intensity and recovery time. Agric. For. Meteorol. 314, 108809. https://doi.org/10.1016/j.agrformet.2022.108809

Zeng, Z., Piao, S., Li, L.Z.X., Wang, T., Ciais, P., Lian, X., Yang, Y., Mao, J., Shi, X., Myneni, R.B., 2018. Impact of Earth greening on the terrestrial water cycle. J. Clim. 31, 2633–2650. https://doi.org/10.1175/JCLI-D-17-0236.1

Zhang, Hao, Ding, J., Wang, Y., Zhou, D., Zhu, Q., 2021. Investigation about the correlation and propagation among meteorological, agricultural and groundwater droughts over humid and arid/semi-arid basins in China. J. Hydrol. 603, 127007. https://doi.org/10.1016/j.jhydrol.2021.127007

Zhang, H., Wu, P., Yin, A., Yang, X., Zhang, M., Gao, C., 2017. Science of the Total Environment Prediction of soil organic carbon in an intensively managed reclamation zone of eastern China : A comparison of multiple linear regressions and the random forest model. Sci. Total Environ. 592, 704–713. https://doi.org/10.1016/j.scitotenv.2017.02.146

Zhang, M., Yuan, X., Otkin, J.A., Ji, P., 2022. Climate warming outweighs vegetation greening in intensifying flash droughts over China. Environ. Res. Lett. 17, 54041. https://doi.org/10.1088/1748-9326/ac69fb

1143 Zhang, X., Chen, N., Li, J., Chen, Z., Niyogi, D., 2017. Multi-sensor integrated
1144 framework and index for agricultural drought monitoring. Remote Sens. Environ.
1145 188, 141–163. https://doi.org/10.1016/j.rse.2016.10.045

1146 Zhang, X., Hao, Z., Singh, V.P., Zhang, Y., Feng, S., Xu, Y., Hao, F., 2022. Drought
1147 propagation under global warming: Characteristics, approaches, processes, and
1148 controlling factors. Sci. Total Environ. 838, 156021.
1149 https://doi.org/10.1016/j.scitotenv.2022.156021

1150 Zhang, X., Zhang, B., 2019. The responses of natural vegetation dynamics to drought
1151 during the growing season across China. J. Hydrol. 574, 706–714.
1152 https://doi.org/10.1016/j.jhydrol.2019.04.084

1153 Zhang, Yu, Hao, Z., Feng, S., Zhang, X., Xu, Y., Hao, F., 2021. Agricultural drought
1154 prediction in China based on drought propagation and large-scale drivers. Agric.
1155 Water Manag. 255, 107028. https://doi.org/10.1016/j.agwat.2021.107028

1156 Zhang, Yao, Keenan, T.F., Zhou, S., 2021a. A global perspective on the probability of
1157 propagation of drought: From meteorological to soil moisture. Nat. Ecol. Evol. 5,
1158 1490–1498. https://doi.org/10.1016/j.jhydrol.2021.126907

1159 Zhang, Yao, Keenan, T.F., Zhou, S., 2021b. Estimating propagation probability from
1160 meteorological to ecological droughts using a hybrid machine learning-Copula
1161 method. Nat. Ecol. Evol. 5, 1490–1498.
1162 https://doi.org/https://doi.org/10.5194/hess-2022-78

1163 Zhang, Yao, Keenan, T.F., Zhou, S., 2021c. Exacerbated drought impacts on global
1164 ecosystems due to structural overshoot. Nat. Ecol. Evol. 5, 1490–1498.
1165 https://doi.org/10.1038/s41559-021-01551-8

1166 Zhao, W., Yu, X., Xu, C., Li, S., Wu, G., Yuan, W., 2022. Dynamic traceability
1167 effects of soil moisture on the precipitation–vegetation association in drylands. J.
1168 Hydrol. 615, 128645. https://doi.org/10.1016/j.jhydrol.2022.128645

1169 Zhao, Z., Wang, H., Yu, C., Deng, C., Liu, C., Wu, Y., Yan, J., Wang, C., 2020.
1170 Changes in spatiotemporal drought characteristics over northeast China from
1171 1960 to 2018 based on the modified nested Copula model. Sci. Total Environ.
1172 739, 140328. https://doi.org/10.1016/j.scitotenv.2020.140328

1173 Zhao, Z., Wang, K., 2021. Capability of Existing Drought Indices in Reflecting
1174 Agricultural Drought in China. J. Geophys. Res. Biogeosciences 126.
1175 https://doi.org/10.1029/2020JG006064

1176 Zhou, Z., Shi, H., Fu, Q., Li, T., Gan, T.Y., Liu, S., 2020. Assessing spatiotemporal
1177 characteristics of drought and its effects on climate-induced yield of maize in
1178 Northeast China. J. Hydrol. 588, 125097.
1179 https://doi.org/10.1016/j.jhydrol.2020.125097

1180 Zhu, Y., Liu, ·Yi, Wang, W., Singh, V.P., Ren, L., 2021. A global perspective on the
1181 probability of propagation of drought: From meteorological to soil moisture. J.
1182 Hydrol. 603, 126907. https://doi.org/10.1016/j.jhydrol.2021.126907

1183

Figure

Click here to access/download;Figure;Fig.1.jpg

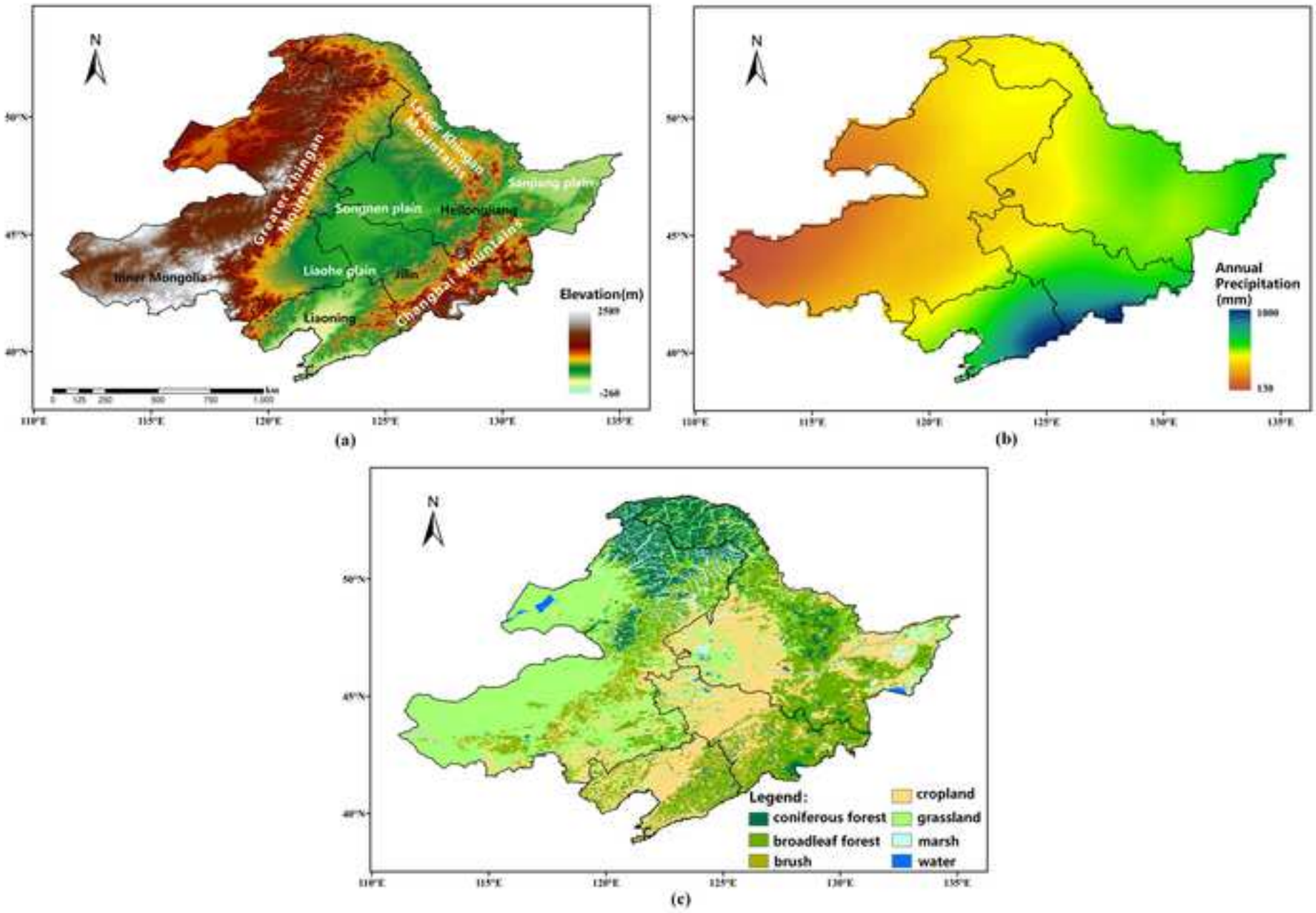

Figure

Click here to access/download;Figure;Fig.2.jpg

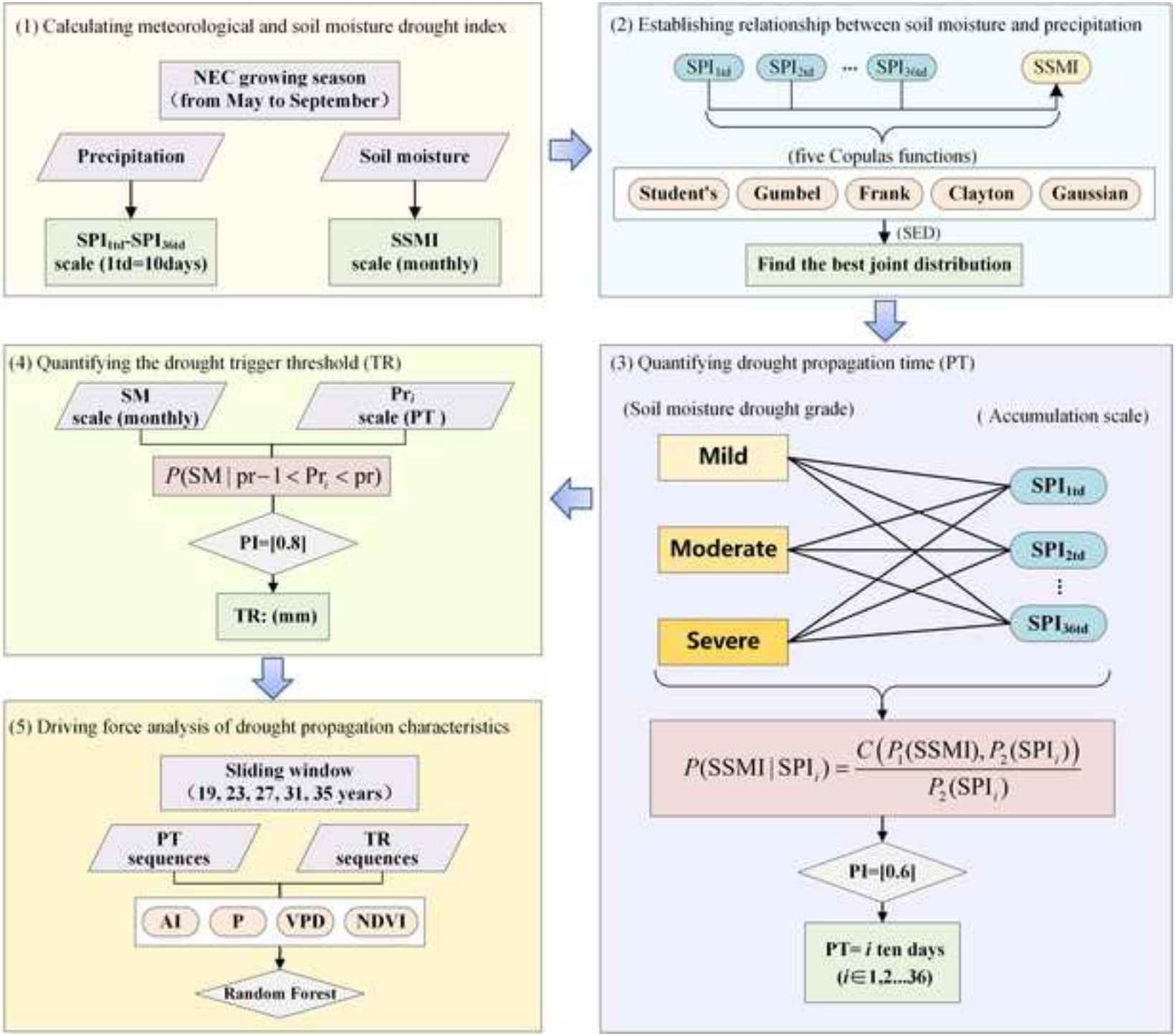

Figure

Click here to access/download;Figure;Fig.3.jpg

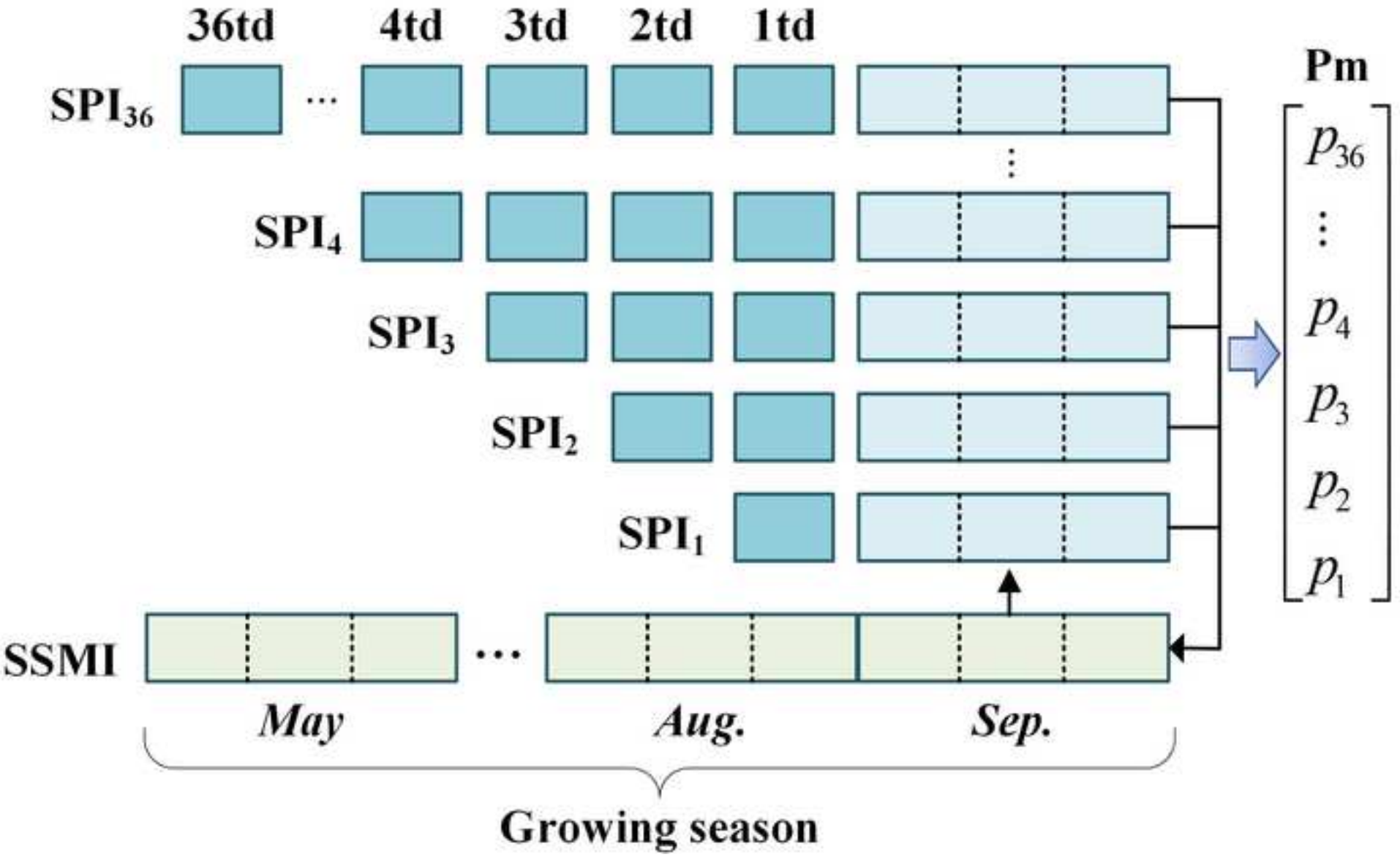

Figure

Click here to access/download;Figure;Fig.4.jpg

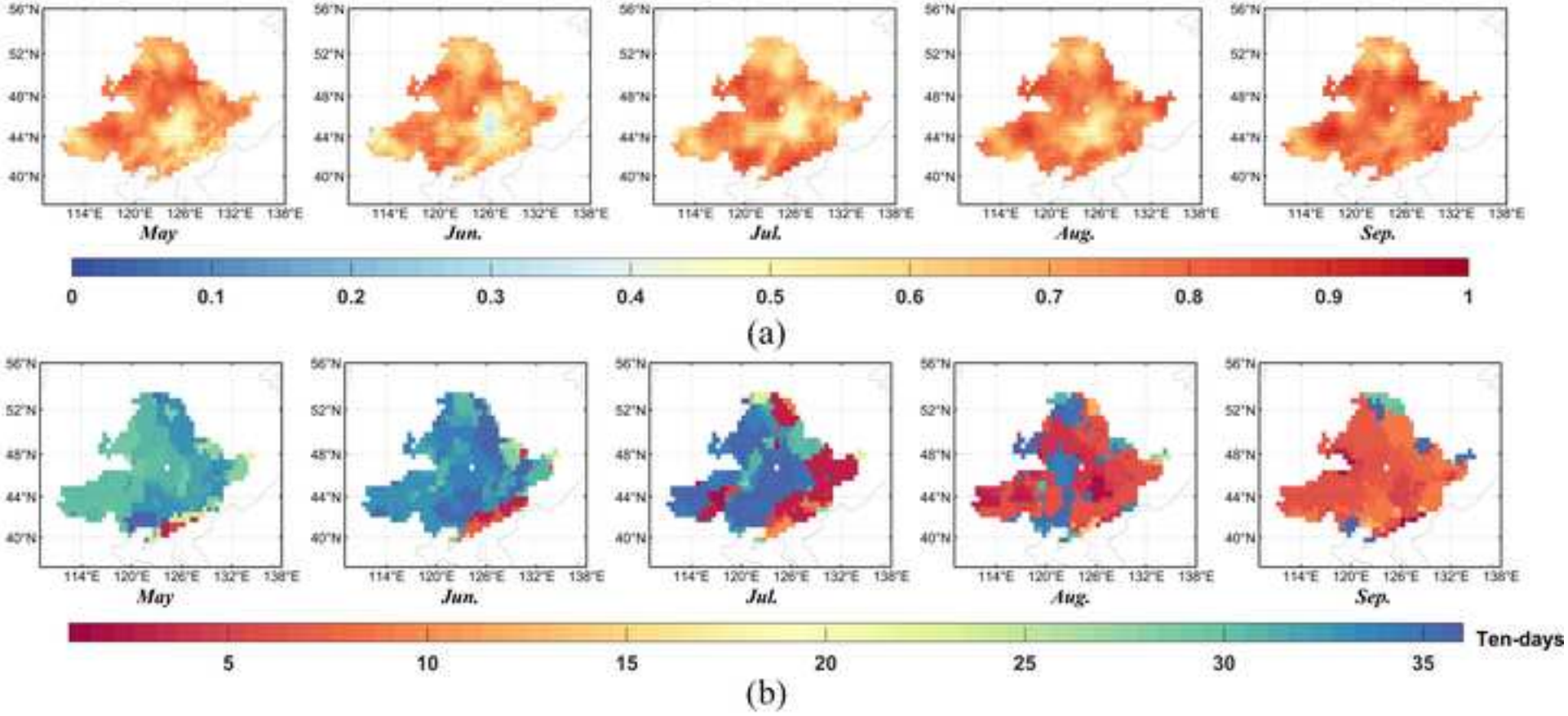

Figure

Click here to access/download;Figure;Fig.5.tif

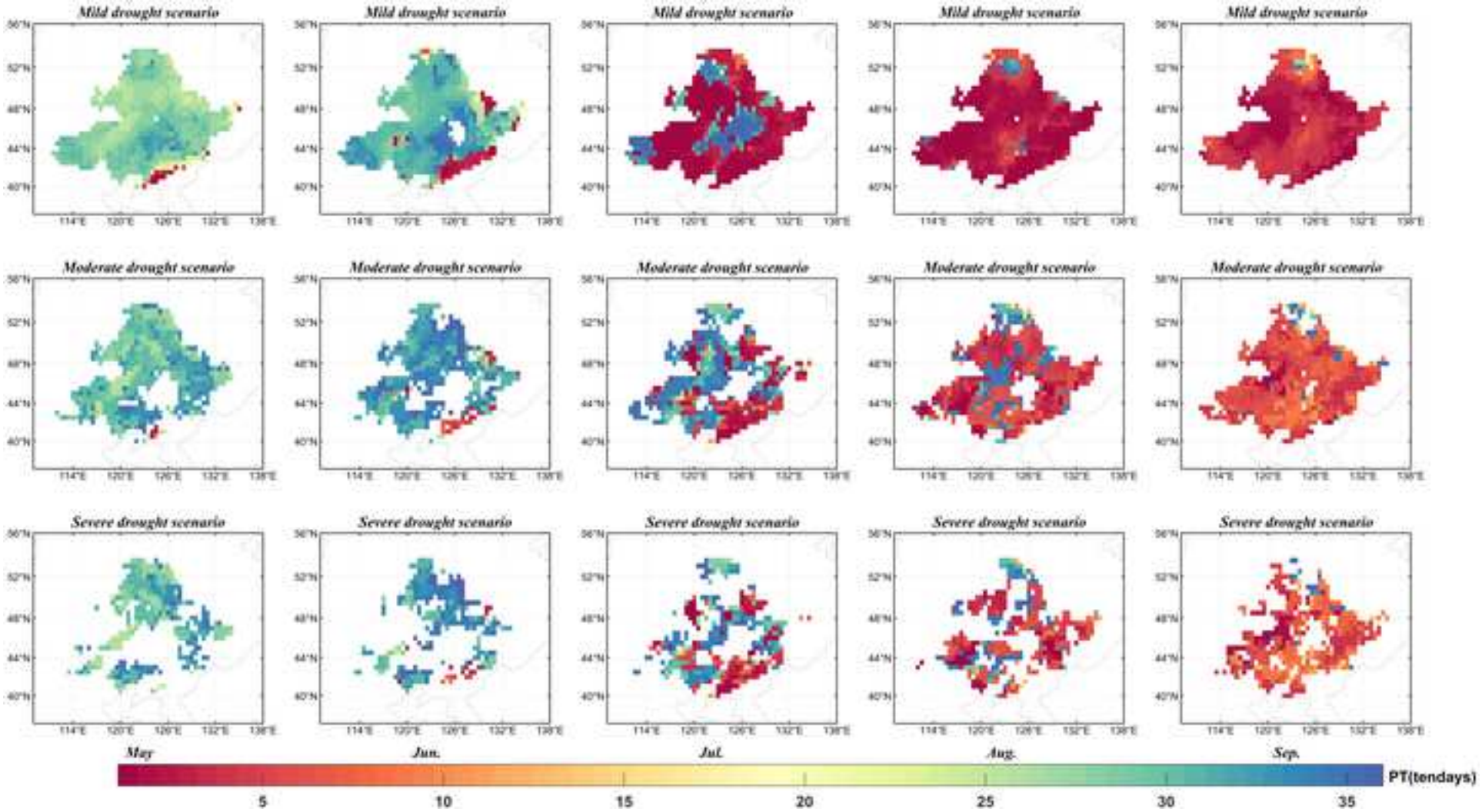

Figure

Click here to access/download;Figure;Fig.6.jpg

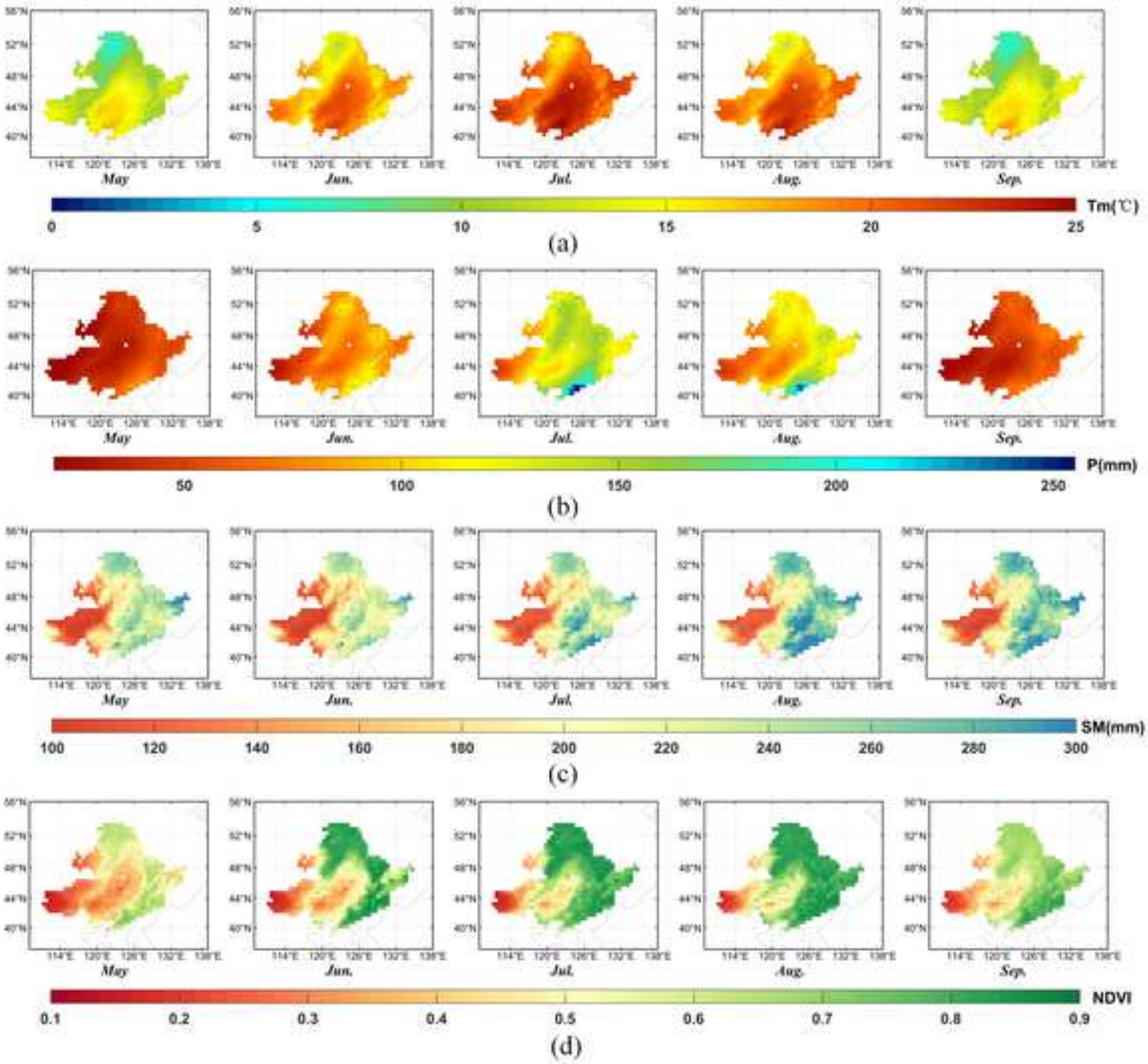

Figure

Click here to access/download;Figure;Fig.7.tif

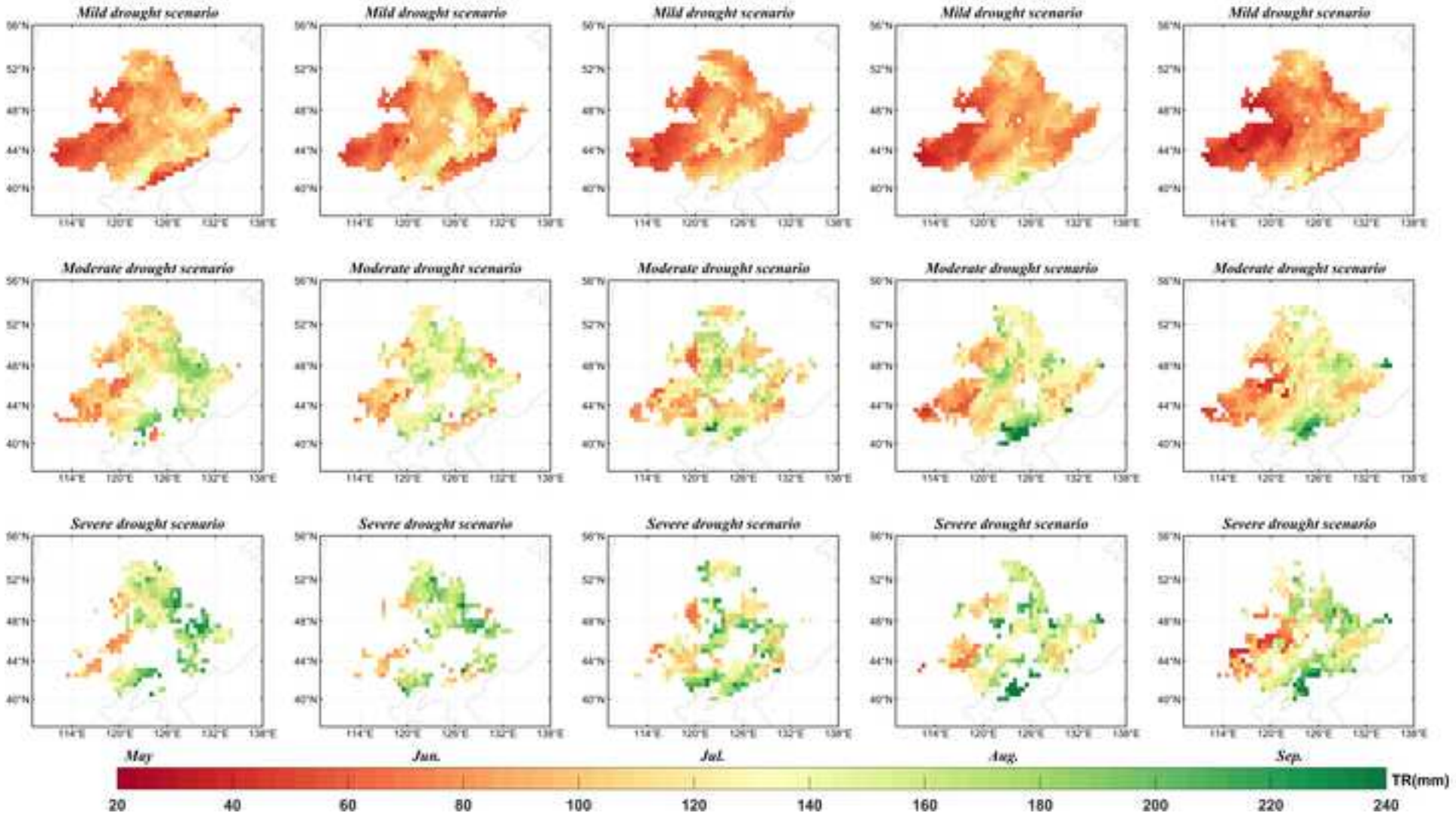

Figure

Click here to access/download;Figure;Fig.8.jpg

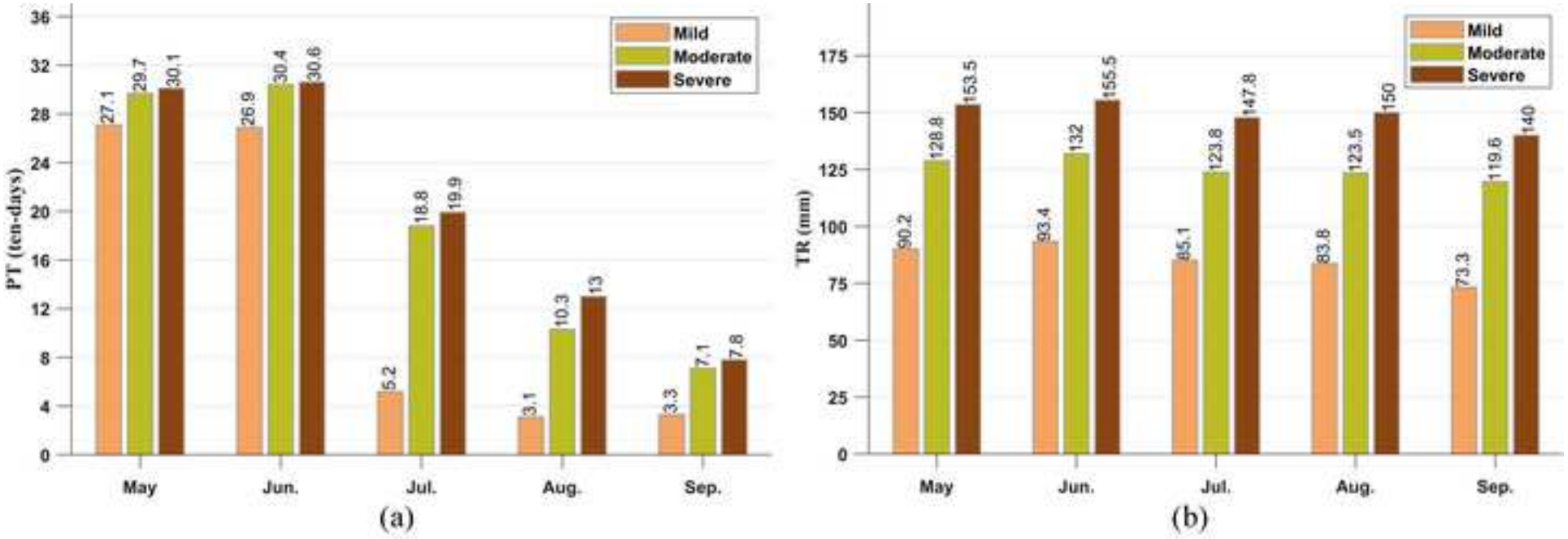

Figure

Click here to access/download;Figure;Fig.9.tif

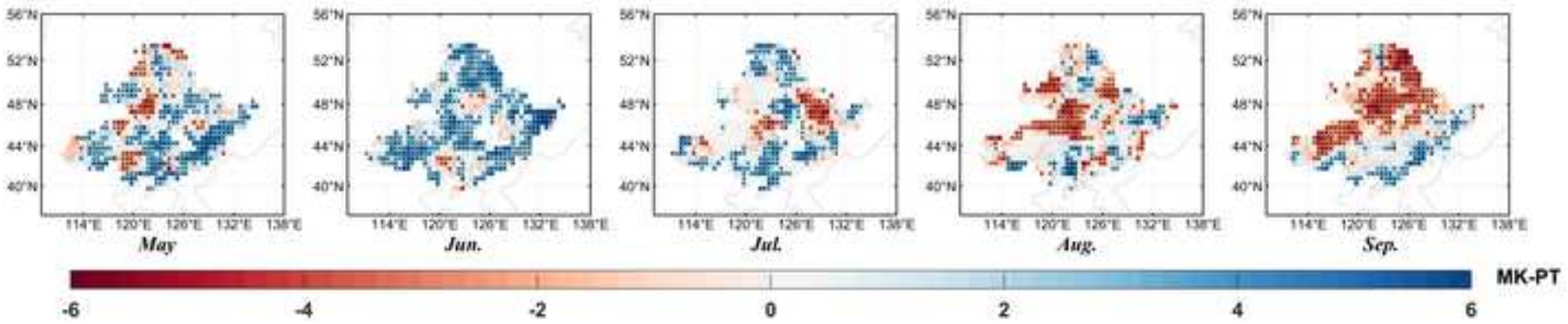

Figure

Click here to access/download;Figure;Fig.10.jpg

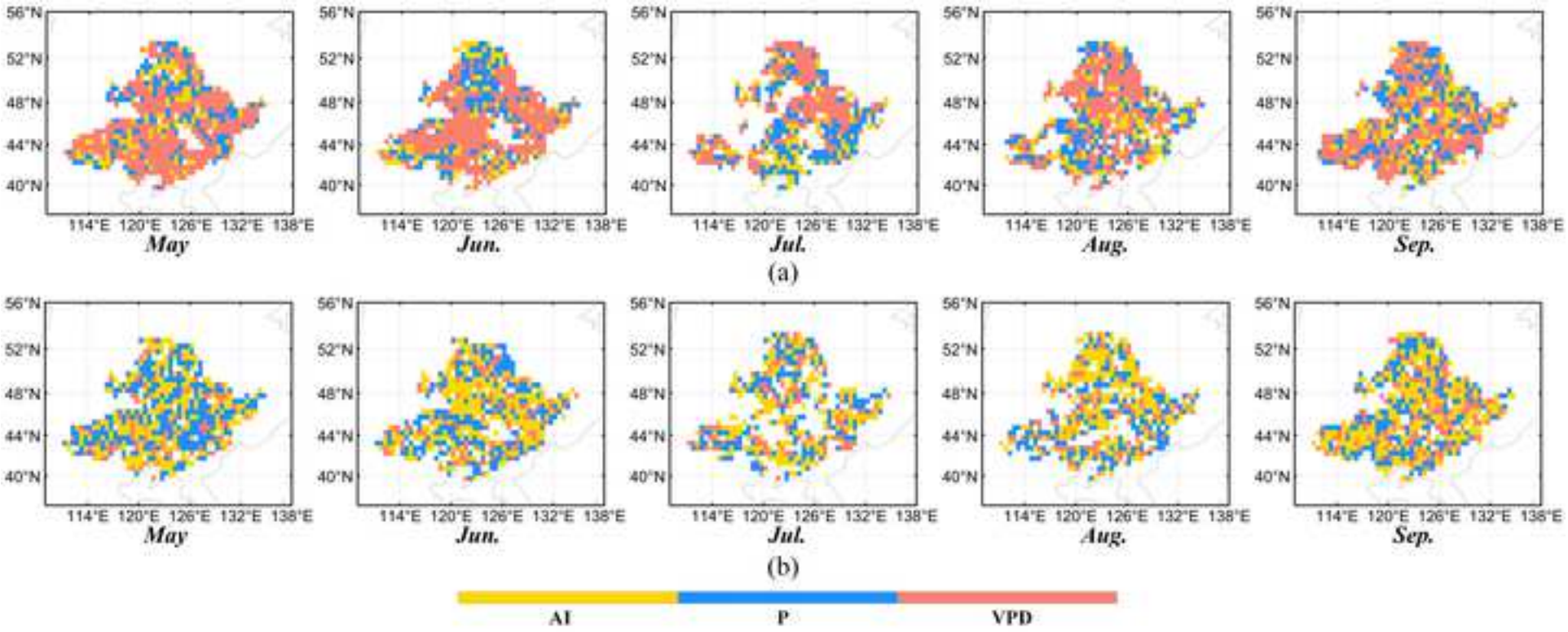

Figure

Click here to access/download;Figure;Fig.11.tif

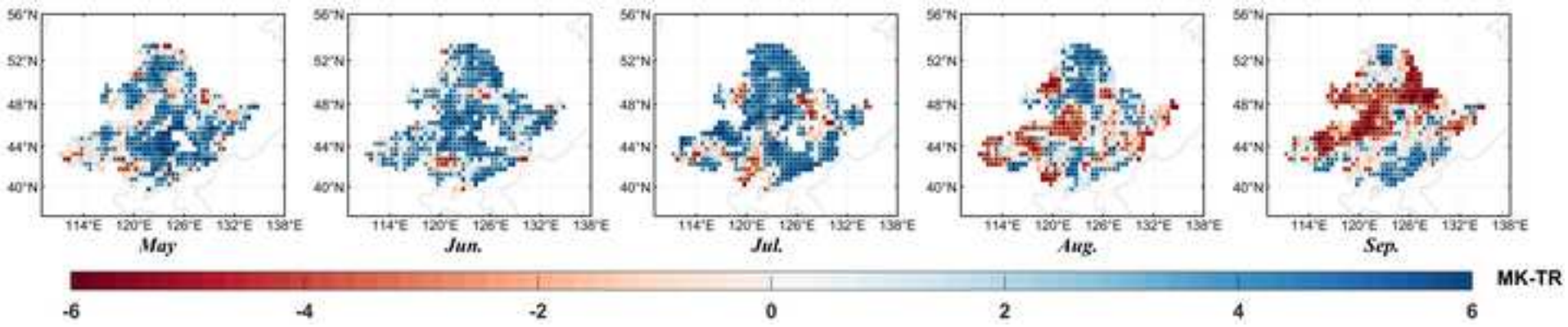

Figure

Click here to access/download;Figure;Fig.12.tif

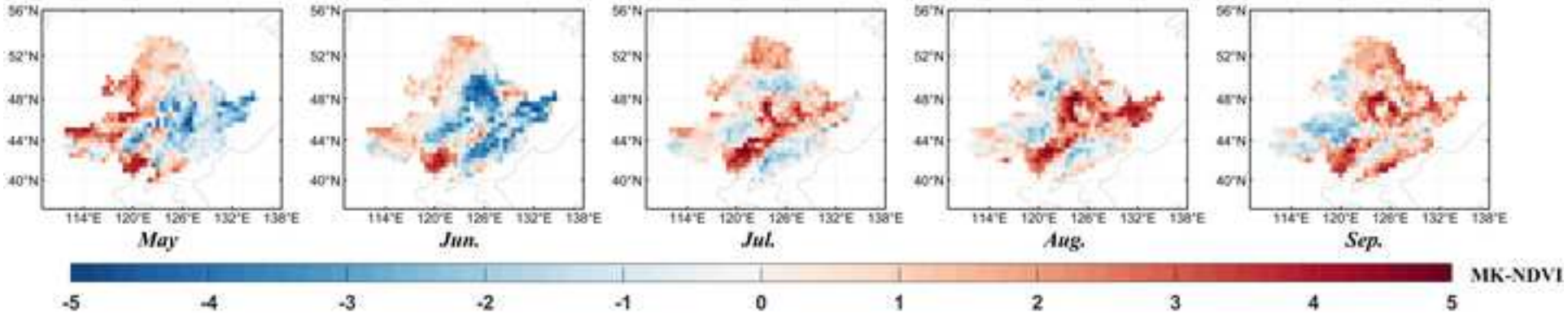

Figure

Click here to access/download;Figure;Fig.13.jpg

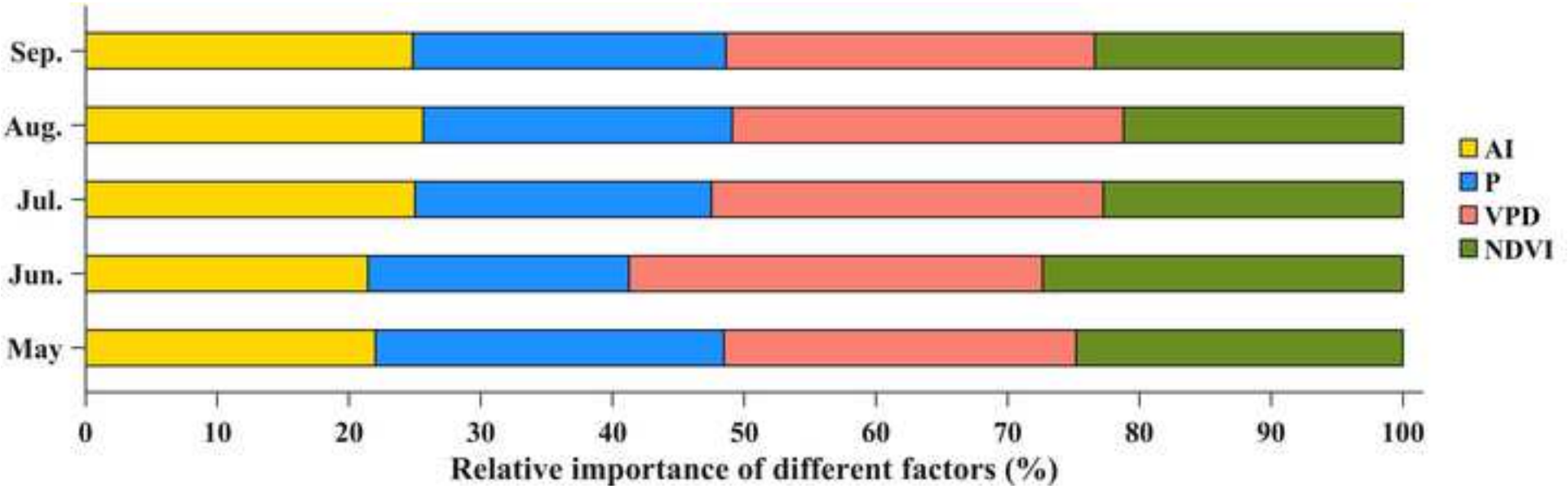

**Table. 1.** Drought classification standard of SPI and SSMI

| Drought grade | SPI/SSMI |
|---|---|
| Mild drought | -1.0 < SPI/SSMI≤-0.5 |
| Moderate drought | -1.5 < SPI/SSMI≤-1.0 |
| Severe drought | -2.0 < SPI/SSMI≤-1.5 |
| Extreme drought | SPI/SSMI≤-2.0 |

**Table. 2.** An overview of the five candidate Copulas

| name | Equation | Generator | Parameter |
|---|---|---|---|
| Clayton | $\max\left(\left[u^{-\alpha}+v^{-\alpha}-1\right]^{-1/\alpha},0\right)$ | $\left(t^{-\alpha}-1\right)/\alpha$ | $\alpha\in(-1,\ \infty)\setminus\{0\}$ |
| Gumbel | $\exp\left(-\left[\left(-\ln u\right)^{\alpha}+\left(-\ln v\right)^{\alpha}\right]^{1/\alpha}\right)$ | $\left(-\ln t\right)^{\alpha}$ | $\alpha\in[1,\infty)$ |
| Gaussian | $\int_{-\infty}^{\phi^{-1}(u)}\int_{-\infty}^{\phi^{-1}(v)}\frac{1}{2\pi\sqrt{1-\rho^2}}\exp\left\{-\frac{s^2-2\rho st+t^2}{2\left(1-\rho^2\right)}\right\}\mathrm{d}s\mathrm{d}t$ | / | $\rho\in(-1,1)$ |
| Frank | $-\frac{1}{\alpha}\ln\left(1+\frac{\left(\mathrm{e}^{-\alpha u}-1\right)\left(\mathrm{e}^{-\alpha v}-1\right)}{\mathrm{e}^{-\alpha}-1}\right)$ | $-\ln\frac{\mathrm{e}^{-\alpha t}-1}{\mathrm{e}^{-\alpha}-1}$ | $\alpha\in(-\infty,\ \infty)\setminus\{0\}$ |
| Student's | $\int_{-\infty}^{t_k^{-1}(u)}\int_{-\infty}^{t_k^{-1}(v)}\frac{1}{2\pi\sqrt{1-\rho^2}}\left[1+\frac{s^2-2\rho st+t^2}{k\left(1-\rho^2\right)}\right]^{-(k+2)/2}\mathrm{d}s\mathrm{d}t$ | / | $\rho\in(-1,1)$ |